Cell Survival miRNAs (29a, 29c, and 221) and Pre-metastatic Prostate Cancer

April Aloway, M.S.[1], Dominique Jones, B.A.[1], Divine Anene [1], Praise Anene, B.S.[1], Diana Avila[1], Leila Gobejishvili [2], Shirsh Barve[1,2], Lacey McNally[1,2] and LaCreis R. Kidd[1]

Department of Pharmacology and Toxicology[1] and Department School of Medicine[2]

University of Louisville School of Medicine

INTRODUCTION

Prostate Cancer (PCa)

- The leading cancer diagnosis American men.
- Indolent PCa is effectively treated with radiation and surgery
- Metastatic disease ,however, has poor survival due to limited treatment options and lack of prognostic tools that predict metastasis.
- Thus, the need to find miRNA that track metastatic disease is imperative.

MiRNAs and their Role in Apoptosis and Cancer

- MiRNAs are responsible for altering the expression of mRNAs that regulate the biological pathways essential to the 6 hallmarks of cancer, including cell survival.
- In particular, overexpression of miR that recognize and inhibit pro-apoptotic mRNA may lead to tumor escape of apoptosis, accumulation of cellular damage, increased proliferation, increased tumor growth and metastasis.
- A few miRNA such as miR34-a, miR125-b, and 488* have been shown as important regulators in cell survival.
  - MiR34-a promotes apoptosis by inhibiting *BCL-2* protein translation preventing bcl-2 mediated degradation of p53.
  - *In vitro and in* vivo studies show that miR125-b works against apoptosis by binding 3 pro-apoptotic genes:*P53, PUMA,* and *Baki*. MiR125 also decreases mitochondrial release of cytochrome C and caspase 3 activity.
  - *In vitro,* MiR488* overexpression decreases tumor growth by decreasing the number of cells that undergo apoptosis.

CLINICAL RELEVANCE

- Detection of serum based miRNAs associated with apoptosis may help to:
  - improve the early prediction of pre-metastatic or metastatic PCa
  - Identify new therapeutic targets for the treatment of metastatic PCa
  - Help clinicians predict patients who may benefit from aggressive PCa treatments.

OBJECTIVE

- To determine whether apoptosis-associated miRNAs are differentially expressed in serum collected from age and race-matched PCa patients with bone-specific metastatic (stage IV), pre-metastatic PCa (stage III), or non-advance disease when compared to disease-free participants (n =5).

HYPOTHESIS

- In comparison to disease-free men, we propose men diagnosed with prostate cancer will have:
  - lower serum levels of miRNA that suppress apoptosis and/or
  - higher levels of miRs that suppress cell death
- We further postulate a stage-dependent expression pattern exists.
  - Specifically, men with more advanced disease will have greater dysregulation as compared to their indolent diseased counterparts.

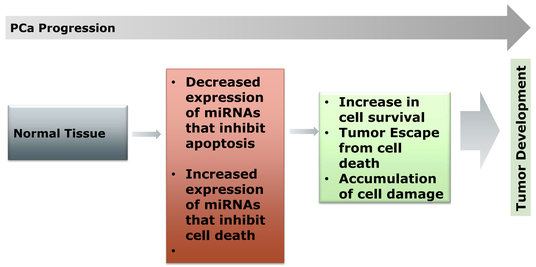

METHODS

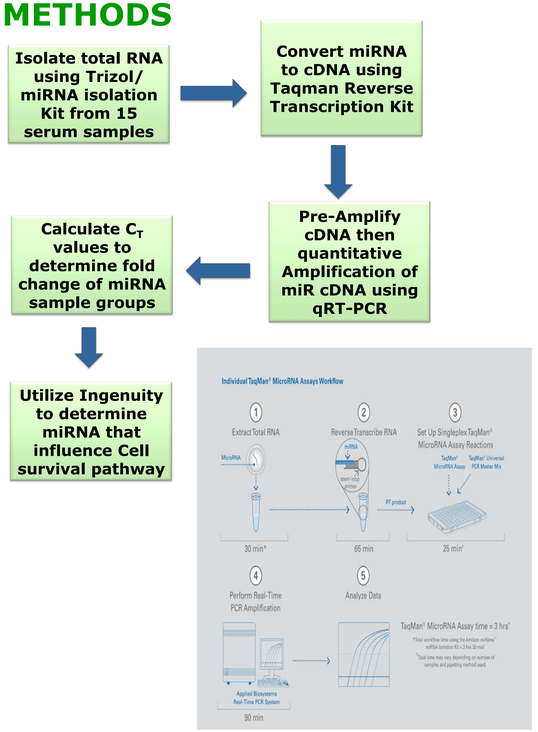

Table 1- Population Characteristics

	Patients	Controls
# Serum samples	15	5
Mean Age (SD), yrs	66.2 (6.46)	66.2 (5.89)
Age Range, yrs	47-72	56-71
Sex, n(%)		
Men	15 (100%)	5 (100%)
Race, n (%)		
Caucasian	15 (100%)	5 (100%)
Smoking, n (%)		
Non-smoker	5 (33.3)	---
Smoker	10 (66.7)	---
PSA		
<4 ng/ml		
≥4 ng/ml	11	5
Missing values	4	
Tumor classification, n(%)		
Adenocarcinoma	9 (60)	
Unknown	6 (40)	

Table 2. Differentially Apoptosis-associated miRNAs in cases and controls

Serum miRNA	P-value	Fold-change (case vs ctrl)	Increased or Decrease in expression	PCa Stage
29c	0.038	2.3	Increase	Stage III
221	0.042	8.1	Increase	Stage III
29a	0.064	0.187	Decrease	Stage IV

Table 3. miRNAs involved in Apoptosis

miRNA	mRNA Target	Source
Let-7c	CASP3, HRAS, TGFBR1, KRAS	Tsang et al., 2008, Oh et al., 2010, Ingenuity
miR-141	TGFB2,TCF4, SOX5	Burk et al., 2008
miR-29c	TNFAIP1,CDC 42	Wang et al. 2011,Park et al. 2009, Ingenuity
miR-221	CASP10, FOS, TBK1	Ichimura et al., 2009, Pineau et al., 2010 Ingenuity
miR-29a	MCL1, CDC42	Lima et al., 2011,Park et al., 2009, Ingenuity

CONCLUSIONS

- Relative to disease-free men
  - miRNAs 221 and 29c were over-expressed by 2.3-8.1 fold in the serum collected from men with Stage III PCA (P = 0.038-0.142).
  - miRNAs 29a had a marginal 81.3% reduction in serum from men with Stage IV disease (P = 0.064)

FUTURE DIRECTIONS

- Future experiments will identify and validate other miRNAs that influence apoptosis using a larger population set.
- Use miRNA mimic or inhibitors *in vitro and in vivo* to elucidate the impact of miRNA- 29a, -29c, and -221 on mRNA targets and PCa bone-specific metastasis.

ACKNOWLEDGEMENTS

NCI R25 Cancer Education Grant to D.W. Hein (CA134283); Our Highest Potential" in Cancer Research Endowment to LRK.

Are Cell Adhesion Associated Micro-RNAs Linked With Metastatic Prostate Cancer?

Divine Anene[1], Dominique Jones [1], April Aloway, M.S.[1], Praise Anene, B.S.[1], Diana Avila[1], Leila Gobejishvili [2], Shirsh Barve[1,2], Lacey McNally[1,2] and LaCreis R. Kidd[1]

Department of Pharmacology and Toxicology[1] and Department School of Medicine[2]
University of Louisville School of Medicine

INTRODUCTION

Prostate Cancer as a Public Health Problem

- Prostate cancer (PCa) remains one of the leading causes of cancer-related deaths among American men.
- In adavnced stages of the disease, metastasis of tumor cells occurs through the process of angiogenesis to the bone.
- Mortality rises markedly as bone metastatic cancers are typically aggressive and often unresponsive to conventional therapy.
- Studies over the last few years have shown the inadequacies associated with the Prostate Specific Antigen (PSA) test, the current gold standard for Pca detection which often fails to adequately detect and stage the disease.
- Solving this problem requires the development of biomarkers that would aid the accurate detection, staging of the disease, and ultimately clinical management of the disease

Micro-RNAs as Effective Cancer Biomarkers

- Limited studies suggest microRNAs (miRNAs) show great promise as PCa biomarkers.
- MiRNAs are small RNA molecules that exert a host of post-transcriptional effects by binding to complementary sequences on messenger RNA (mRNA) transcripts resulting in translational repression, target degradation, and gene silencing.
- Their relative stability and resistance to RNase degradation in addition to the ease with which they are detected in biological samples make them great prognostic tools for Pca metastasis.
- While several studies have been done with tissues and other cell lines, very little work has been done with serum which could provide a less invasive means of detecting disease.

OBJECTIVES

- To determine whether cell adhesion associated miRNAs are differentially expressed in serum collected from age and race-matched PCa patients with bone-specific metastatic (stage IV), pre-metastatic PCa (stage III), or non-advance disease when compared to disease-free participants (n =5).

Hypothesis

- We hypothesized that individuals with advanced stage PCa would have lower levels of miRNAs that influence cell adhesion.

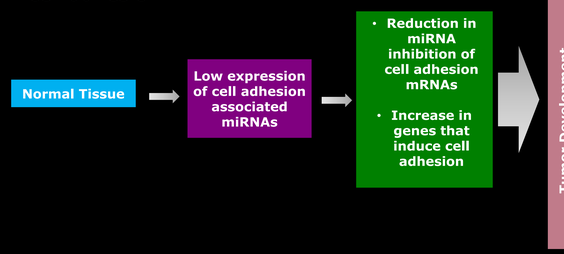

CLINICAL RELEVANCE

- The findings of our study may serve as a foundation to for future studies to identify and validate miRNA as non-invasive biomarkers for bone specific PCa metastasis.
- The establishment of biomarkers that track with pre-metastatic and metastatic PCa will help guide new aggressive treatment strategies toward individuals susceptible to metastatic disease.
- Ultimately, investigation of these biomarkers will improve early detection of pre-metastatic and metastatic PCa in patients.

METHODS

Step 1
- Separation of serum into 250 µl aliquots
- Denaturation of serum using TriZol Reagent LS
- Isolation of total RNA using miRNA miRVana Isolation Kit

Step 2
- Quantitation of Total RNA using a Nanodropper
- miRNA selection using In Silico tools(Ingenuity, KEGG, BioCarta)

Step 3
- Serum miRNA profile expression analysis (Taqman Array Human miRNA cards)
- Data analysis

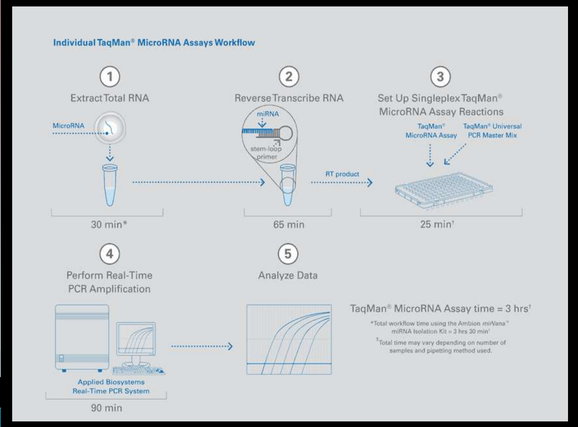

Table 2. Differentially expressed serum miRNAs in cases and controls

Serum miRNA	P-value	Fold-change (case vs ctrl)	Increase/ Decrease in expression	Disease Stage Comparisons
185	0.204	7.82	Increase	Stage I vs. Controls
29a	0.064	0.187	Decrease	Stage IV vs. Controls
133a	0.198	0.026	Decrease	Stage IV vs. Controls
145	0.074	0.094	Decrease	Stage IV vs. Controls
197	0.064	0.136	Decrease	Stage IV vs. Controls

Table 3. miRNAs involved in Cell Adhesion using Ingenuity

Pathway	miRNA	mRNA Targets
Cell Adhesion		
	let-7a	CCND1
	128	TGFBR1
	129-5p	SOX4
	132	RB1
	133a	CASP9
	143	BCL2, KRAS
	145	MYC
	146a	CHUK
	149	E2F1
	155	TCF7L2
	195	BCL2, CCND1, WNT3A, ZYX
	185	CDC42, RHOA
	18a	CDKN1A, E2F1
	193a-3p	CCND1
	197	ACVR1, TSPAN3
	219-5p	PLCG2
	222	CDKN1B, DIRAS3, PIK3R1, PTEN
	26a	PTEN
	29a	ARPC3, CDC42, PIK3R1
	34a	BCL2, CCND1, CREB1, HDAC1
	375	PDPK1
	200b	PLCG1

Table 1. Characteristics of study population

	Patients	Controls
# Serum samples	15	5
Age		
Range	47-72	56-71
Mean (SD)	66.2 (6.46)	66.2 (5.89)
Sex, n(%)		
Men	15 (100%)	5 (100%)
Race, n (%)		
Caucasian	15 (100%)	5 (100%)
Smoking, n (%)		
Non-smoker	5 (33.3)	NA
Smoker	10 (66.7)	NA
PSA		
<4 ng/ml		
≥4 ng/ml	11	5
Missing values	4	
Tumor classification, n(%)		
Adenocarcinoma	9 (60)	
Unknown	6 (40)	

CONCLUSIONS

Relative to disease-free individuals:

- Several cell adhesion-associated miRNAs detected in the serum of patients with stage IV disease were down-regulated
  - miRNAs-133a, 197 as well as miRNAs-145 and 29a, which were marginally significant (P-value = 0.064-0.074).
- However, one cell adhesion-associated miRNA detected in the serum of patients with stage I disease was up-regulated
  - miRNA-185, but it was not significant.
- Overall the cell adhesion-associated miRNAs found in the study were down-regulated among men w/ bone-specific metastasis.

FUTURE DIRECTIONS

- We will validate differentially expressed serum miR targets individually using Taqman Singleplex miRNA assays.
- Determine miR and mRNA signatures using archival tissue.
- Use miR mimics and inhibitors to determine whether miRNAs regulate the expression of mRNAs that regulate cell migration, motility or metastasis.
- Establish a co-culture bone metastasis model to determine whether miRNA inhibitors/mimics will modify: adhesion of tumor cells to bone; bone cell's susceptibility to tumor invasiveness, or release of chemokines, growth hormones, or osteoporin.

ACKNOWLEDGEMENTS

Grant/Research Support: NCI R25 Cancer Education Grant to D.W. Hein (CA134283); Our Highest Potential" in Cancer Research Endowment to LRK.

Utilizing the Humoral Response to Early-stage Lung Cancer as a Potential Biomarker for Early Diagnosis

James Bradley, Kavitha Yaddanapudi, Ph.D, Sharon Willer, Jason Chesney, M.D., Ph.D.[1,2], John W. Eaton, Ph.D.

Department of Medicine

University of Louisville School of Medicine

Introduction

Lung cancer is the major cause of cancer-related deaths worldwide, accounting for about 1.3 million deaths annually. Approximately $10.3 billion is spent on lung cancer treatment in the United States each year. Often, clinical symptoms only appear during later stages of cancer, or a diagnosis is made after an x-ray is done for other medical reasons. Various screening strategies have been tested for detection of early stage lung cancer but only one cumbersome technique (low-dose computed tomography) has shown any significant reduction in lung cancer mortality. Though this method can detect smaller nodules than conventional CT scans, there is also an associated high number of false-positives, necessitating additional tests.[1] Autoantibodies have been found in patient serum up to five years before spiral CT scans were able to detect non-small cell lung cancer nodules, suggesting the possibility of earlier detection via autoantibodies.[2]

We have developed an inexpensive and fast alternative blood test that we believe will detect antibodies that appear early in the development of lung cancer. The test involves flow cytometric analyses of A549 (human lung adenocarcinoma) cells incubated with dilute patient serum and a secondary anti-human IgG antibody (tagged with the fluorescent tag, R-Phycoerythrin).

In very early tests of this system, we found that two of four serum samples from stage I non-small cell lung cancer patients were positive for antibodies against A549 cells. Additional tests with samples from later stages of lung cancer development have confirmed that antibodies can be detected throughout lung cancer stages 1-3.
A potential strength of this approach is that it is a broad-spectrum screen that will identify antibodies against a variety of cell surface antigens. In addition to detecting lung cancer in its earliest stages, our technique also offers the exciting possibility of identifying novel human lung cancer antigens, extracellular as well as intracellular, that may serve as targets for future therapy.

Materials & Methods

Extracellular Antigen Detection

1) Grow 1x10^5 A549 human adenocarcinoma cells in 100 ul staining buffer (PBS + 1% Fetal Bovine Serum). Add human serum to a final dilution of 1:50 and incubate on ice for 30 minutes.
2) Wash cells twice at 1500 RPM for 5 minutes with 2 ml of staining buffer.
3) Add anti-human IgG, F_C fragment specific (conjugated with PE) to a final dilution of 1:100 and incubate on ice for 30 minutes in the dark.
4) Wash cells twice with 2 ml of staining buffer.
5) Resuspend cells in 500 ul of staining buffer and test for antibody binding via flow cytometry.

Intracellular Antigen Detection

1) Grow up 1x10^5 A549 human adenocarcinoma cells and incubate in 100 ul fixing solution for 30 minutes at room temperature.
2) Wash with 2 ml of permeabilization buffer (diluted 1:10 in dH_2O).
3) After washing, add human serum to a final dilution of 1:50 and incubate for 30 minutes at room temperature.
4) Follow steps 2-5 of the extracellular protocol described below except use permeabilizationbuffer instead of the staining buffer and all steps should be conducted at room temperature.

Theoretical Framework behind Autoantibody Detection

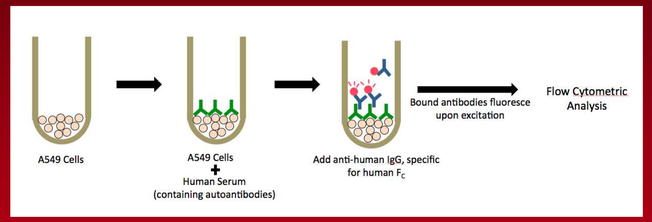

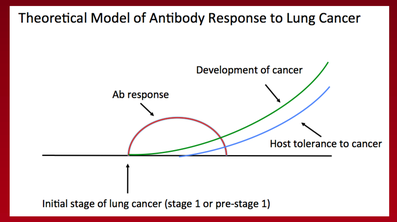

Results

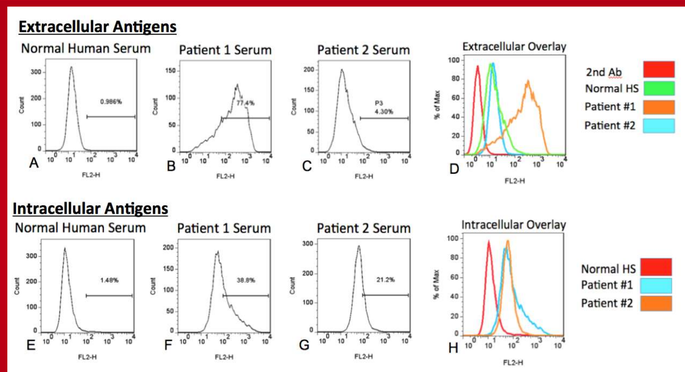

Figure 1. Detection of autoantibodies via flow cytometry using an anti-human IgG antibody, specific for F_C, indicates the production of IgG antibodies in early stage lung cancer. Results from the initial experiment (n=4) indicate that it is possible to detect autoantibodies against non-small cell lung cancer in 50% of the serum samples using our novel method of detection. The results also show that extracellular antigens (A-D) as well as intracellular antigens (E-H) can be detected.

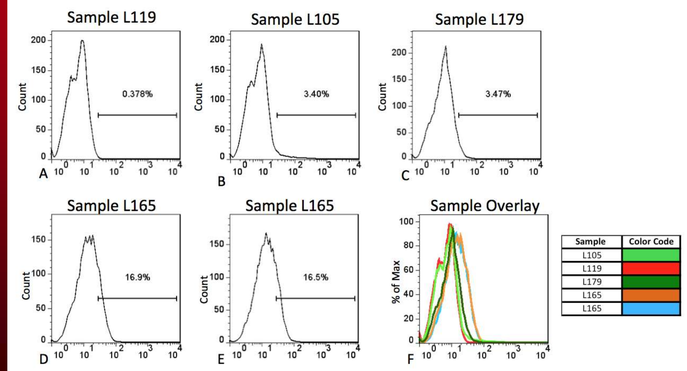

Figure 2. Detection of autoantibodies in later stages of non-small cell lung cancer reveals a lower titer of antibodies present in human serum during later stages of cancer development. Results from additional testing (n=15) indicate that antibodies are detectable in some (A-D), but not all serum samples. There is also evidence of reproducibility within samples (D-E).

Table 1. Percent Positive Cells for autoantibody binding from early stage lung cancer serum to extracellular/intracellular antigens on A549 cells.

		Extracellular	Intracellular
Serum Sample	Stage of Cancer	% Cells Positive	% Cells Positive
Normal	N/A	0.986	1.480
Patient 1	1	77.400	38.800
Patient 2	1	4.300	21.200

Table 2. Percent Positive Cells for autoantibody binding from late-stage lung cancer serum to extracellular antigens on A549 cells.

		Extracellular
Serum Sample	Stage of Cancer	% Cells Positive
L105	2	3.400
L119	3	0.378
L179	3	3.470
L165	3	16.900
L165	3	16.500

Conclusions

The results indicate that it is possible to detect autoantibodies in early, as well as late, stages of non-small lung cancer development that react to antigens found on the surface of A549 (human lung adenocarcinoma) cells using an anti-human IgG antibody. As seen in Fig. 1A, background from normal human serum is low compared to autoantibodies that can be detected in the serum from a patient with stage 1 lung cancer (Fig. 1B). Although it is evident that there is variability in antibody response as detected by our system (50% of serum samples from stage 1 did not register a response), we believe this phenomenon could be explained by the repression of MHC class I molecules on tumor cell surfaces. This currently remains to be validated due to the difficulty of acquiring paired serum/tissue samples from patients diagnosed with non-small cell lung cancer.

Repeated tests on several samples (Figs. 2D-2E and other samples not shown) have confirmed that the results are reproducible within the samples. This suggests that the reason for the variability between samples from the same stages (Figs. 1B-1C [stage 1], and Figs. 2A, 2C, 2D [stage 2]) remains to be elucidated. Tests on additional serum samples will provide a more comprehensive overview of the IgG response that can be detected with our method. Higher dilutions of serum have been tested (data not shown) which resulted in a reduced response from the cancer patient serum, but not in the normal serum. This suggests that specific, rather than non-specific, binding is occurring between the autoantibodies and the extracellular antigens on A549 cells.

Our results indicate that our technique allows the detection of intracellular antigens (Figs. 1E-1H) as well as extracellular antigens (Figs. 1A-1D). This method presents the exciting possibility of being able to identify novel cancer antigens that may serve as targets for future drug development.

Future Work and Limitations

The limitations of this method include the inability to detect autoantibodies from non-small cell lung cancer patients in which the cancerous cells have lost their MHC class I molecules. It has been shown that about 38% of non-small cell lung cancer tissues will lose their MHC class I molecules.[3] Further complicating this technique, it is difficult to properly analyze the decrease in autoantibody response throughout the four stages of lung cancer development without previous knowledge of the degree to which the cancer cells have begun to repress MHC class I molecule expression.

Future work will include testing additional serum samples that we currently have access to as well as testing all samples against an IgM secondary antibody to determine if class switching may be occurring during the early stages of cancer. We intend on further searching for serum samples from sources that include information on MHC class 1 molecule status (present or absent) or for paired serum/tissue samples. In the future, we also intend on identifying and isolating novel cancer antigens using this technology via proteomics approaches.

References

1. Bach, Peter B., MD, *et al*. "Benefits and Harms of CT Screening for Lung Cancer." *Journal of the American Medical Association* 307.22 (2012): 2418-429.
2. Zhong, Li, PhD, *et al*. “Profiling Tumor-Associated Antibodies for Early Detection of Non-small Cell Lung Cancer.” *Journal of Thoracic Oncology* 1.6(2006): 513-519.
3. Korkolopoulou, P., L. Kaklamanis, F. Pezzella, A. L. Harris, and K. C. Gatter. "Loss of Antigen-presenting Molecules (MHC Class I and TAP-1) in Lung Cancer." *British Journal of Cancer* 73 (1996): 148-53.

Acknowledgements

Research supported by a grant from University of Louisville Cancer Education Program NIH/NCI (R25-CA134283)

Gene Expression in Breast Carcinomas from Patients with Ethnical Differences

Adrienne M. Bushau, Sarah A. Andres and James L. Wittliff

Department of Biochemistry & Molecular Biology, Brown Cancer Center and Institute for Molecular Diversity & Drug Design, University of Louisville, Louisville, KY 40292

Abstract:

Background: African American women often exhibit more aggressive breast cancer and have a higher mortality rate than Caucasian women. Differences in cultural and socioeconomic status are possible explanations for the higher mortality rate and more advanced stage of breast cancer. However, numerous studies suggest that differences in insurance coverage and socioeconomic status do not explain the observed differences observed in clinical behavior of breast carcinomas of black and white patients, suggesting a biological basis. The goal was to ascertain if dissimilarities occur in gene expression of breast carcinoma biopsies of white and black patients, and further to evaluate if these gene expression differences were related to cancer behavior.

Materials and Methods: Using an IRB-approved biorepository and database, gene expression levels were compared in tissue biopsies from white and black patients utilizing microarray analyses of LCM-procured breast carcinoma cells and assessed with clinical information. These studies generated a candidate gene list, which included TRAPPC2L, CRYBB2P1 and PDHA1 to be validated by qPCR. Then frozen tissue sections from de-identified patients diagnosed with primary breast carcinoma and metastasis were utilized. Total RNA was extracted from frozen intact tissue sections with the RNeasy® Mini Kit (Qiagen Inc.). Integrity of RNA was analyzed using the Bioanalyzer 2100 (Agilent Technologies). Total RNA was reverse transcribed using iScript (Biorad). Primers were designed using Primer Express (Applied Biosystems) and Primer Blast (NCBI). RNA quantification and analyses were performed in triplicate by qPCR in duplicate wells using the ABI Prism® 7900HT (Applied Biosystems) with Power Sybr® Green (Applied Biosystems) for detection. Relative gene expression was calculated using the ΔΔCt method with cDNA prepared from Universal Human Reference RNA (Stratagene) as both a calibrator and a standard for quantification of RNA using β-actin (ACTB) as a reference gene. T-tests, box and whisker and Kaplan-Meier plots were performed in Graph Pad Prism. Pearson correlations and Cox regressions were performed in SPSS Statistics 20. The gene interactions were evaluated with Ingenuity IPA.

Results: Examination of candidate gene expression levels from microarray analyses revealed that CARD11 (P=0.001), TRAPPC2L (P<0.001), CRYBB2P1 (P<0.0001) and PDHA1 (P<0.0001) exhibited significant differences in breast carcinomas of African American patients compared to those of Caucasian patients. Of these genes, only PDHA1 expression was correlated with overall survival (P=0.05) when the entire population of 245 breast carcinoma patients was stratified by median gene expression level without regard to race. Only PDHA1 expression assessed by microarray was correlated with overall survival (P=0.04) of white patients when stratified by race and gene expression level. From the expression levels of 20 genes found most significant by T-test of the microarray data, PDHA1, CRYBB2 and TRAPPC2L were investigated further by qPCR. Using a platform comparison of gene expression levels of candidate genes from qPCR and microarray, CRYBB2 was significantly correlated (P=0.01), while PDHA1 was insignificantly correlated (P=0.22). From analyses of tumor marker protein results, significant differences were detected in estrogen and progestin receptor gene expression levels in tissue biopsies when comparing white and black patients and white and hispanic breast carcinoma patients.

Conclusions: Expression levels of CARD11, PDHA1, TRAPPC2L and CRYBB2P1 were significantly different in breast tissue biopsies of African American patients when compared to those of Caucasian patients. Of the four genes, only PDHA1 gene expression levels of LCM-procured carcinoma cells were significant when correlated with overall survival of the entire population (n=245) regardless of race. Furthermore, PDHA1 expression was correlated with overall survival when only white patients were considered. Although dissimilarities in gene expression levels were observed in black and white patients, preliminary evaluation of a limited gene subset to personalize prognosis assessment requires additional studies related to a patient's ethnical background.

Introduction:

Numerous studies have shown that African American women often have a more aggressive breast cancer and have a higher mortality rate than Caucasian women. A difference in cultural and socioeconomic status is one explanation for African Americans presenting a higher mortality rate and a more advanced stage of breast cancer than Caucasian patients. However, some studies have shown that differences in insurance coverage and socioeconomic status do not explain the observed differences seen between blacks and whites (1). Through this information, it is valid to suspect biological differences affecting breast cancer in black and white patients. Breast tumors may be classified using five immunohistochemical (IHC) tumor markers: estrogen receptor (ER), progesterone receptor (PR), and human epidermal growth factor receptor-2 (HER2) (2). Estrogen and progesterone receptors play an important role in predicting prognosis and response to endocrine therapy in breast cancer. Hormone receptor-negative breast tumors are associated with poorer survival, whereas tumors that have a lobular history are associated with better survival (1). Almost two thirds of ER- positive patients respond favorable to endocrine therapy; less than ten percent of ER-negative patients exhibit a favorable response to endocrine therapy (1). Previous studies have shown that African Americans are more likely to have ER-negative, PR-negative breast tumors (2). This study primarily focused on the discrepancies in gene expression involved in white and black breast cancer patients.

Materials and Methods

Tissue Preparation & RNA Extraction

Using an IRB-approved study, frozen tissue sections from de-identified patients diagnosed with primary breast carcinoma and metastasis were utilized. Total RNA was extracted from frozen intact tissue sections with the RNeasy® Mini Kit (Qiagen Inc., Valencia, CA). Integrity of RNA was analyzed using the Bioanalyzer 2100 (Agilent Technologies, Palo Alto, CA). Total RNA was reverse transcribed using iScript (Biorad, Hercules, CA).

Gene Expression Analyses

Primers were designed using Primer Express (Applied Biosystems) and Primer Blast (NCBI). RNA quantification and analyses were performed in triplicate by qPCR in duplicate wells using the ABI Prism® 7900HT (Applied Biosystems, Foster City, CA) with Power Sybr® Green (Applied Biosystems) for detection. Relative gene expression was calculated using the ΔΔCt method with cDNA prepared from Universal Human Reference RNA (Stratagene, La Jolla, CA) as both a calibrator and a standard for quantification of RNA using β-actin (ACTB) as a reference gene.

Statistical Analysis

T-test, Kaplan Meier Plots, and Tumor Marker Analyses were performed in Graph Pad Prism. Pearson Correlations were performed in SPSS Statistics 20. The Gene Interactions were performed through Ingenuity IPA.

Figure 1: Kaplan-Meier Plots of Black vs White Patients without Regard to Gene Expression Levels

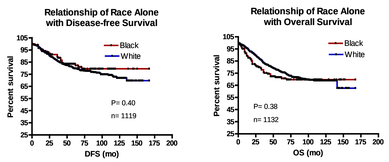

Figure 2: Box and Whisker Plots of Tumor Marker Levels of Patients with Differing Ethnical Heritage

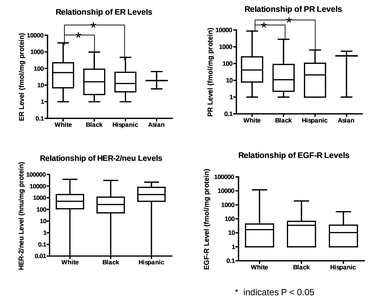

* indicates P < 0.05

Table 1: Results of T-Test of Microarray Data Comparing Gene Expression Levels in Patients with Differing Racial Backgrounds

(Most Significant Genes are Shown)

Gene ID	T-test (P-value)
PSPH	7.07 E-11
TRAPPC2L	5.36 E-10
PCSK4	4.61 E-08
DPH2	4.18 E-07
CARD11	4.87 E-07
SLIT3	5.90 E-07
PLEKHA8	9.12 E-07
PDHA1	9.37 E-07
CRYBB2P1	9.37 E-07
HAMP	9.78 E-07
SLC22A1	1.20 E-06
CST5	1.39 E-06
DCSTAMP	1.53 E-06
GLS2	2.67 E-06
WDR48	2.87 E-06
A4GNT	4.68 E-06
CGB1	4.88 E-06
KRTAP3-3	5.60 E-06
POLRIA	5.66 E-06
PNO1	8.02 E-06

Figure 3: Box and Whisker Plots of Expression Levels of Candidate Genes from Microarray

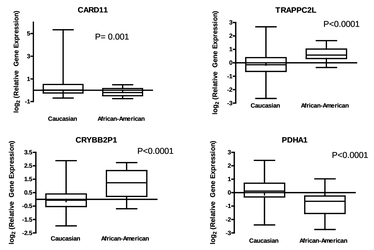

The box represents gene expression levels within the second and third quartiles of values observed. The horizontal line within the box represents the median expression level, while the whiskers extend to the lowest and highest expression level for each gene.

Figure 4: Kaplan-Meier Plots of Patients Stratified by Levels of Expression of the Candidate Genes without Regard to Race (n = 245)

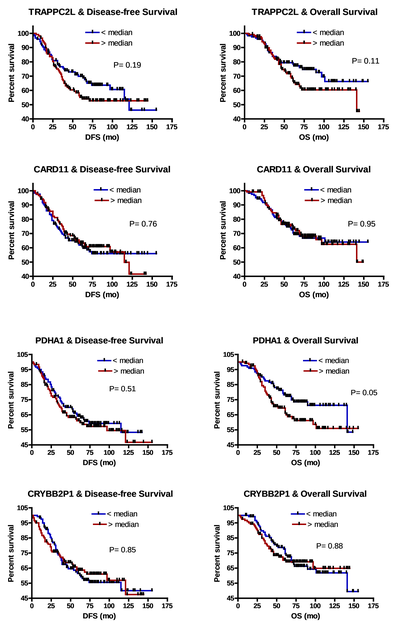

Figure 5: Kaplan-Meier Plots of Patients Stratified by Levels of Expression of the Candidate Genes & Patient Race (n = 245)

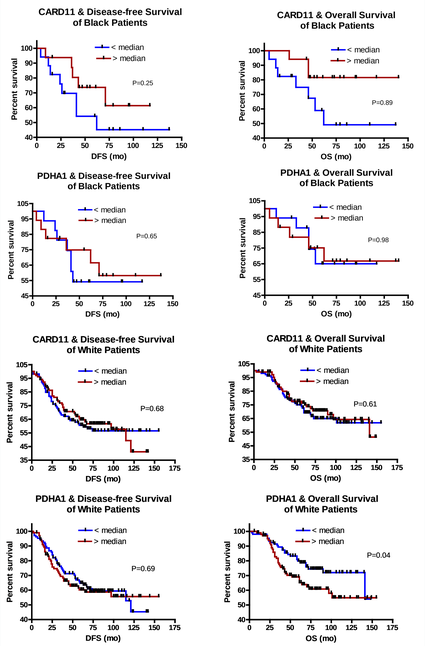

Figure 6: Comparison of Expression Levels of Candidate Genes Measured by Microarray and qPCR (n = 46)

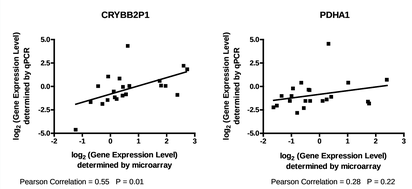

Figure 7: Kaplan-Meier Plots of Patient Survival in Relation to Gene Expression Levels Measured by qPCR (n = 46)

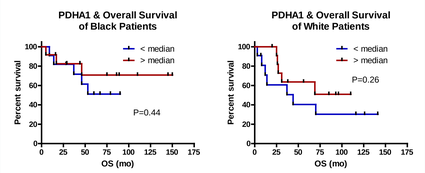

Figure 8: Gene Interactions Identified using Ingenuity Pathway Analysis (Genes of Interest indicated by Shaded Areas)

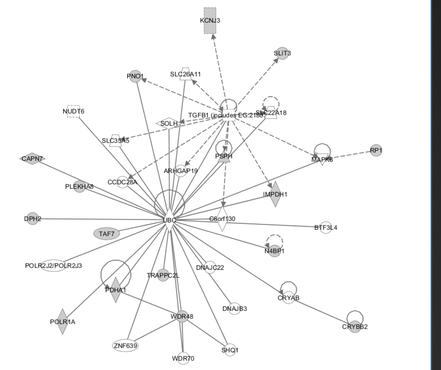

Conclusions:

- Patient survival did not appear to be correlated with race when the overall population was considered (n = 1132).
- ER and PR protein levels were significantly different in carcinomas of white, black and hispanic patients, but no differences were observed in HER-2/neu or EGF-Receptor protein levels.
- Comparisons of gene expression levels in breast carcinomas from patients with different ethnical backgrounds identified 475 genes with P < 0.01 and 116 genes with P < 0.001 using microarray data.
- Candidate genes from microarray data were analyzed further: CARD11, PDHA1, TRAPPC2L and CRYBB2P1 expression levels were significantly different in tissue biopsies when compared to patient ethnical heritage.
- PDHA1 gene expression in LCM-procured carcinoma cells was significantly correlated with overall survival of the study population regardless of race.
- PDHA1 expression in LCM-procured carcinoma cells was correlated with overall survival only in white patients.
- CARD11, TRAPPC2L and CRYBB2P1 expression did not appear to be correlated with patient survival in patients of different ethnical heritage.
- Gene expression was also evaluated by qPCR in a subset of patients for further analysis.
- Evaluation of a limited gene subset suggests additional studies are warranted to determine the relationship of a breast cancer patient's ethnical background to personalize prognosis assessment.

References:

1. Li CI et al. Differences in Breast Cancer Hormone Receptor Status and Histology by Race and Ethnicity among Women 50 Years of Age and Older. Cancer Epidemiol Biomarkers Prev 11:601-607, 2002.
2. O'Brien KM et al. Intrinsic Breast Tumor Subtypes, Race, and Long-term Survival in the Carolina Breast Cancer Study. Clin Cancer Res 16: 6100-6110, 2010.
3. Ma XJ et al. Gene expression associated with clinical outcome in breast cancer via laser capture microdissection. Breast Cancer Res Treat 82, 2003.
4. Mohla S et al. Estrogen and Progesterone Receptors in Breast Cancer in Black Americans: Correlation of Receptor Data with Tumor Differentiation. Cancer 50:552-9, 1982.
5. Wittliff JL et al. Gene expression profiles and tumor marker signatures of human breast carcinoma cells procured by laser capture microdissection. Endocrine Soc Abs P3-198, 2002.
6. Wittliff JL et al. Expression of estrogen receptor-associated genes in breast cancer cells procured by laser capture microdissection. Jensen Symp Abs 81, 2003.

Acknowledgements:

AMB was supported by a fellowship from the NCI R25 grant support University of Louisville Cancer Education Program NIH/NCI (R25-CA134283).

In Silico Screening for Novel Human Arylamine *N*-Acetyltransferase 1 Inhibitors

Samantha M. Carlisle, B.S.[1,3], Carmine S. Leggett, Ph.D.[1,3], John O. Trent, Ph.D.[2,3], Mark A. Doll, M.S.[1,3], J. Christopher States, Ph.D.[1,3], David W. Hein, Ph.D.[1,3]
Department of Pharmacology and Toxicology[1], Department of Medicine[2], James Graham Brown Cancer Center[3]
University of Louisville School of Medicine
Louisville, KY 40202

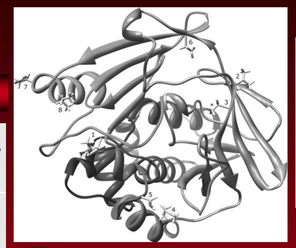

Ribbon diagram of human NAT1 enzyme

Abstract

Human arylamine *N*-acetyltransferase 1 (NAT1) is a phase II xenobiotic-metabolizing enzyme that plays an important role in the deactivation and bioactivation of many environmental carcinogens such as, 4-aminobiphenyl (ABP) which is found in cigarette smoke. Arylamines, such as ABP can either be *N*-acetylated (deactivation) by NAT1, or if first acted upon by a cytochrome P450 enzyme, they can be *O*-acetylated (bioactivated) by NAT1. Once bioactivated, these compounds form arylnitrenium ions leading to DNA adducts. If not repaired by nucleotide excision (NER), these DNA adducts can lead to mutagenesis and cancer initiation. Human NAT1 is therefore an ideal molecular target for cancer therapy. Compound 10, an effective inhibitor of human NAT1 was previously discovered using *in silico* screening. This compound has been shown to decrease human NAT1 activity, ABP-induced DNA adducts, cell proliferation, and cell invasion in human breast adenocarcinoma cells. The objective of this project was to identify novel small molecule inhibitors of human NAT1 that were even more potent than compound 10 by building upon the previous *in silico* studies through the utilization of an updated ZINC library and also by performing a similarity search to compound 10. The two new *in silico* searches performed identified 161 potential NAT1 inhibitors, 35 of which were tested for their ability to inhibit human NAT1 *in vitro*. From this initial screening, compounds 63, 66, 72, 86, and 95 were chosen as lead compounds because they experimentally inhibited human NAT1 greater than 75% *in vitro*. We determined the IC_{50} values of these lead compounds to be 66.1, 5.74, 161, 100, and 102 μM, respectively. The most potent inhibitor, compound 66, was chosen for further experiments. Compound 66, inhibited human NAT1 recombinantly expressed in yeast (*in vitro* IC_{50} = 5.57 μM) and endogenously expressed in human breast cancer cells (*in situ* IC_{50} = 2.44 μM). Compound 66 was tested against human NAT2 (*in vitro* IC_{50} = 12.8 μM) to determine which isozyme of NAT it preferentially binds to, with the results showing a preference for human NAT1, our molecular target. [NCI R25-CA134283]

Hypothesis

Inhibition of human NAT1 activity will decrease carcinogen metabolism and cancer progression.

Objective

- To identify potent novel small molecule inhibitors of the molecular target human NAT1 that will suppress carcinogen activation and cancer progression.

Introduction

- Human arylamine *N*-acetyltransferase occurs in two isozymes, NAT1 and NAT2. These isozymes bioactivate environmental carcinogens such as 4-aminobiphenyl (ABP).
- Human NAT1 is a proposed molecular target for novel small molecule inhibitors because it has been found to be overexpressed in urinary bladder, breast, colorectal, and lung cancers. This overexpression has been linked to enhanced growth properties and etoposide (cancer medication) resistance in human breast cancer cells. Here, we describe the identification of novel and effective NAT1 inhibitors.

Methods

- Two *in silico* searches for small molecule inhibitors that bind to the active site of human NAT1 were performed.
- The *in silico* screening program Surflex-Dock 2.3 was used to conduct a virtual search that screened small molecule inhibitors that had been added to the ZINC library since the previous search had been conducted. Sixty-five compounds were identified in the virtual search as potential inhibitors, scored, and ranked based on their active site association.
- The *in silico* screening program Surflex-Sim was used to conduct a similarity search that screened compounds that were structurally similar to compound 10, a small molecule inhibitor that was discovered in a previous screening and was found to be an effective inhibitor of human NAT1. Ninety-seven compounds were identified in the similarity search as potential inhibitors, scored, and ranked based on their active site association.
- Based on their commercial availabilities, 35 compounds were tested for their ability to inhibit NAT1 activity. The IC_{50} values of the most efficacious inhibitors (compounds 63, 66, 72, 86, and 95) were determined *in vitro* against human NAT1.
- Further studies were completed using the most potent inhibitor of the lead compounds, compound 66.

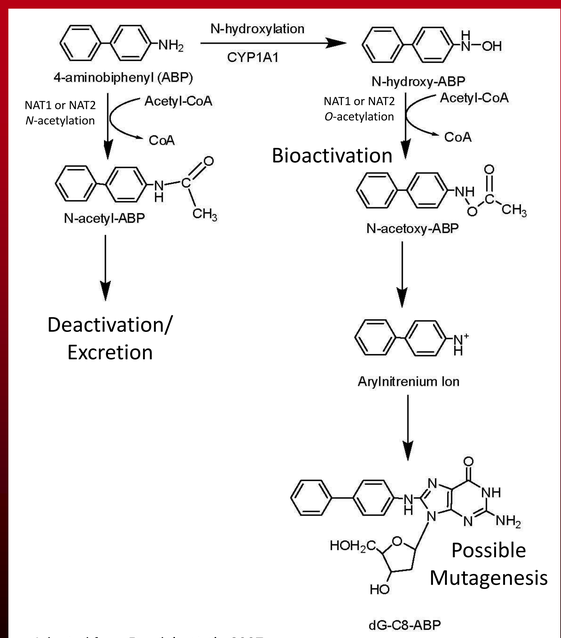

Adapted from Bendaly et al., 2007.

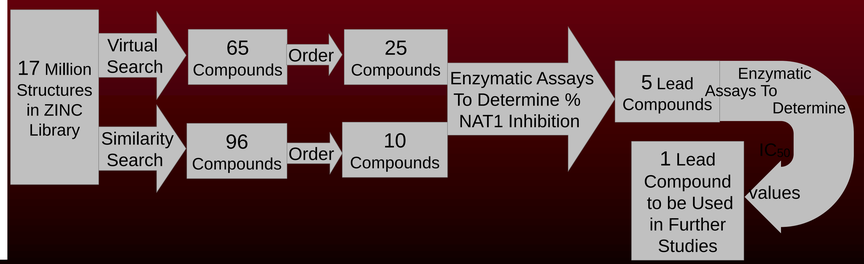

Results

Compound #	Screening Source	% NAT 1 Inhibition
61	Virtual	0.00%
62	Virtual	40.4%
63	**Similarity**	**89.2%**
64	Similarity	32.6%
65	Similarity	46.1%
66	**Similarity**	**93.1%**
67	Virtual	14.3%
68	Virtual	0.00%
69	Virtual	33.3%
70	Virtual	23.8%
71	Virtual	38.1%
72	**Similarity**	**78.1%**
73	Virtual	0.00%
74	Similarity	13.9%
75	Similarity	35.3%
76	Virtual	12.7%
77	Virtual	0.00%
78	Virtual	0.00%
79	Virtual	0.00%
80	Virtual	0.00%
81	Virtual	0.00%
82	Virtual	21.5%
83	Virtual	0.00%
84	Similarity	0.00%
85	Virtual	70.1%
86	**Virtual**	**76.8%**
87	Virtual	0.00%
88	Virtual	27.6%
89	Virtual	0.00%
90	Virtual	4.7%
91	Similarity	70.9%
92	Virtual	32.2%
93	Virtual	0.00%
94	Similarity	55.4%
95	**Virtual**	**79.4%**

***TABLE 1*: Percent inhibition of human NAT1 activity *in vitro*. The compounds in red inhibited human NAT1 activity greater than 75%.**

Compound #	*In vitro* NAT1 IC_{50} (μM)
63	66.1 ± 7.56
66	**5.74 ± 1.05**
72	161 ± 43.6
86	100 ± 9.56
95	102 ± 17.0

***TABLE 2*: Lead compounds IC_{50} *in vitro* against human NAT1 (PABA). The compound in red is the most potent, and therefore used for further experiments.**

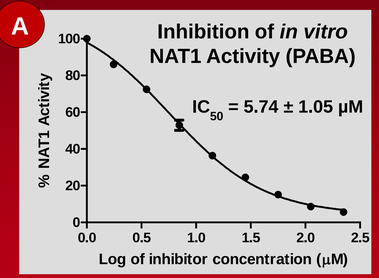

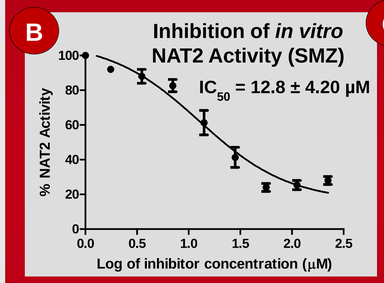

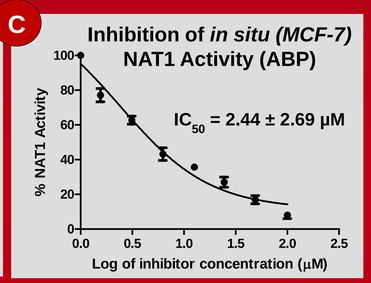

FIGURES A-C: *A*. *In vitro* NAT1 activity was determined using 100 μM acetyl coenzyme A and 300 μM p-aminobenzoic acid (PABA) with varying concentrations of compound 66 (0 – 100 μM) in yeast lysates that express recombinant human NAT1. *B*. *In vitro* NAT2 activity was determined using 100 μM acetyl coenzyme A and 300 μM sulfamethazine (SMZ) with varying concentrations of compound 66 (0 – 100 μM) in yeast lysates that express recombinant human NAT2. C. In situ NAT1 capacity was determined in human breast cancer cells (MCF-7) that express endogenous NAT1. These cells were treated with media supplemented with 6.67 μM ABP or PABA with varying concentrations of compound 66 (0 – 100 μM). Reaction products were collected and analyzed using high pressure liquid chromatography (HPLC) to determine the amount of acetylated product.

Conclusions

- We have identified 5 novel inhibitors of human NAT1 and have experimentally determined their IC50 values *in vitro*.
- Based on these data, compound 66, is the most effective and potent NAT1 inhibitor. Compound 66 was also an effective inhibitor of endogenous NAT1 activity in MCF-7 (human breast cancer cells) using in situ assays. These data show promising results for further studies.
- Further *in situ* studies are needed using compound 66, to evaluate the compounds ability to inhibit cell invasion, proliferation, and also metastasis which are all hallmarks of cancer.

Acknowledgements

Partially supported by the University of Louisville Cancer Education Program (NCI R25-CA134283).

Echinomycin Decreases Cell Viability of Pancreatic Adenocarcinoma Cells through Inhibition of Autophagy

J. Brett Farmer[1], Justin S. Huang[2], Lacey R. McNally[2]

[1] Middle Tennessee State University, [2] Department of Medicine, University of Louisville

ABSTRACT

Objective: Pancreatic carcinomas are the fourth leading cause of cancer death in the United States. Because pancreatic cancers respond poorly to conventional chemotherapy, investigation of new drug treatment options is needed. We hypothesized that echinomycin, an inhibitor of hypoxia-inducible factor-1 (HIF-1), would significantly decrease cell viability of pancreatic cancer cell lines in a hypoxic environment.

Methods: Highly metastatic pancreatic adenocarcinoma cell lines S2VP10 and S2CP9 and the non-metastatic pancreatic adenocarcinoma cell line MiaPaCa2 were treated with echinomycin in normoxic (20% O_2) and hypoxic (5% O_2) conditions. Following treatment with 1 nM, 5 nM, 10 nM, 20 nM, and 40 nM echinomycin, cell viability after 24 hours, as a measure of ATP, was compared to an untreated normoxic control in all cell lines. Mechanism of induced cell death by echinomycin was evaluated using cell stress and apoptosis profiling. Proteins from treated cell lines and untreated control cell lines were harvested and analyzed by western blotting to evaluate changes in the autophagy pathway.

Results: In all three cell lines treated with 10 nM of echinomycin, cell viability at twenty-four hours was less than 50% in comparison to the normoxic control. Accumulation of prominent autophagosomes was evident in treated cell lines twelve hours after treatment. Cell stress array revealed a prominent increase in heat shock protein 60 (HSP60) in treated S2VP10 cells in comparison to untreated S2VP10 cells. Although apoptosis array revealed extremely high levels of pro-caspace-3, cleaved caspace-3 did not increase in treated S2VP10 cells. In all treated cell lines, levels of the autophagy marker protein light chain 3-II (LC3-II) were greatly increased in comparison to untreated cell lines.

Conclusion: Our results indicate that echinomycin inhibits cell viability of metastatic pancreatic cancer cells through inhibition of autophagy rather than through apoptosis. Treatment with echinomycin in a hypoxic environment resulted in higher levels of cellular death in comparison to normoxic conditions. Echinomycin has potential to be used in combination drug therapy as a treatment for pancreatic adenocarcinoma.

MATERIALS AND METHODS

Cell Lines

Highly metastatic pancreatic adenocarcinoma cell lines S2VP10 and S2CP9 and the non-metastatic cell line MiaPaCa2 were maintained in RPMI or DMEM cell culture medium supplemented with 1% L-Glutamine and 10% FBS.

Treatment and Cell Viability

Cells were treated with 1 nM, 5 nM, 10 nM, 20 nM, and 40 nM of echinomycin and incubated in normoxic (20% oxygen) and hypoxic (5% oxygen) conditions. Following treatment for 24 hours, cell viability, as a measure of ATP, was compared to an untreated normoxic control in all cell lines with an ATPLite™ Luminescence Assay System.

Protein analysis

The mechanism of induced cell death under hypoxic conditions for untreated S2VP10 control cells and S2VP10 cells treated with echinomycin for 24 hours was then evaluated using R&D Systems human cell stress array and apoptosis arrays in untreated S2VP10 control cells and S2VP10 cells treated with 5 nM (cell stress array) or 10 nM (apoptosis array) echinomycin for twenty-four hours under hypoxic and normoxic conditions. Proteins from untreated control cell lines and cell lines treated with 10 nM echinomycin for twelve and twenty-four hours were harvested. Proteins harvested after twenty-four hours of echinomycin treatment were analyzed for the autophagy marker protein LC3-II by Western blotting. Proteins harvested after 12 hours of echinomycin treatment were analyzed by Western blotting for both the LC3-II protein and the autophagy marker protein autophagy protein five (Atg-5).

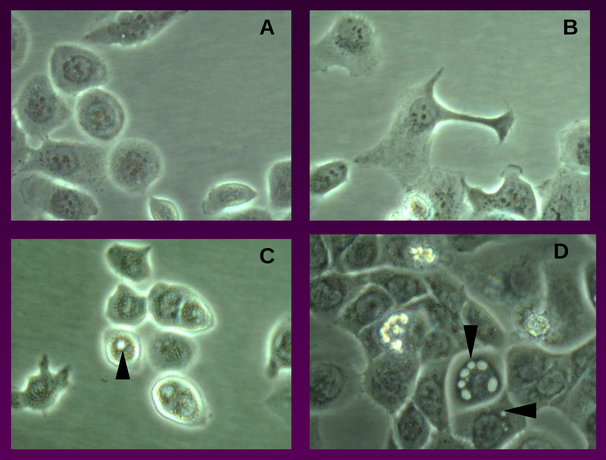

Figure 1. Cellular morphology 12 hours after echinomycin treatment.
Untreated S2VP10 cells in normoxic conditions, 20% oxygen, (A) or hypoxic condtions, 5% oxygen, (B) after twelve hours. S2VP10 cells treated with 10 nM echinomycin in normoxic conditions (C) or hypoxic conditions (D) after twelve hours. Black arrows indicate the presence of prominent autophagosomes.

Results

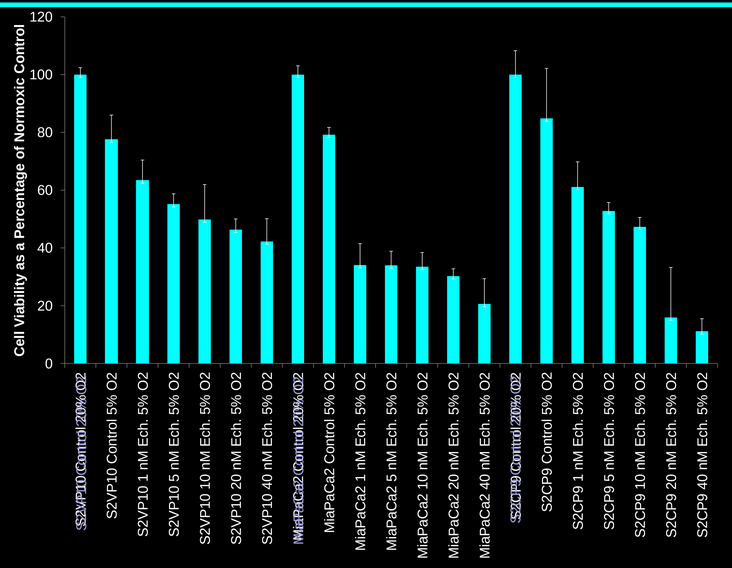

Figure 2. Cell viability after 24 hours of echinomycin treatment.
S2VP10, S2CP9, and MiaPaCa2 cells treated with echinomycin or untreated control cells were placed in both normoxic (20% oxygen) and hypoxic (5% oxygen) conditions for twenty-four hours. Viability of cells placed in hypoxic conditions, as a measure of ATP, was compared to an untreated normoxic control in all cell lines.

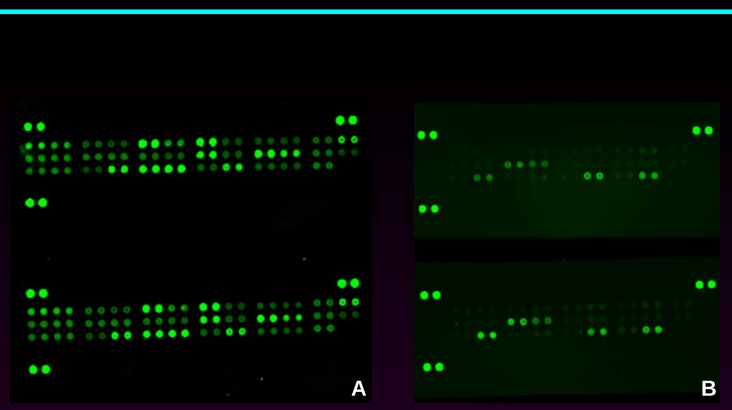

Figure 3. Human apoptosis array (A) and cell stress array (B) membranes.
Proteins harvested from untreated control S2VP10 cells in hypoxic conditions and S2VP10 cells treated with 10 nM echinomycin for twenty-four hours in hypoxic conditions were incubated on nitrocellulose membranes containing binding sites for thirty-five different apoptosis-related proteins. (B) Proteins harvested from untreated control S2VP10 cells in hypoxic conditions and S2VP10 cells treated with 5 nM echinomycin for twenty-four hours in hypoxic conditions were incubated on nitrocellulose membranes containing binding sites for twenty-six cell stress related proteins.

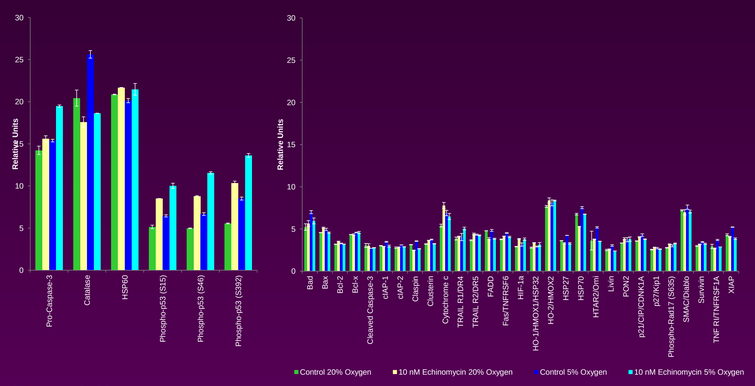

Figure 4. Human apoptosis array.
Proteins harvested from untreated S2VP10 control cells placed in both normoxic and hypoxic conditions for 24 hours and S2VP10 cells treated with 10 nM echinomycin for 24 hours in both normoxic and hypoxic conditions were incubated on nitrocellulose membranes containing binding sites for thirty-five different apoptosis related proteins. Relative levels of proteins were compared to standard reference spots on the membranes.

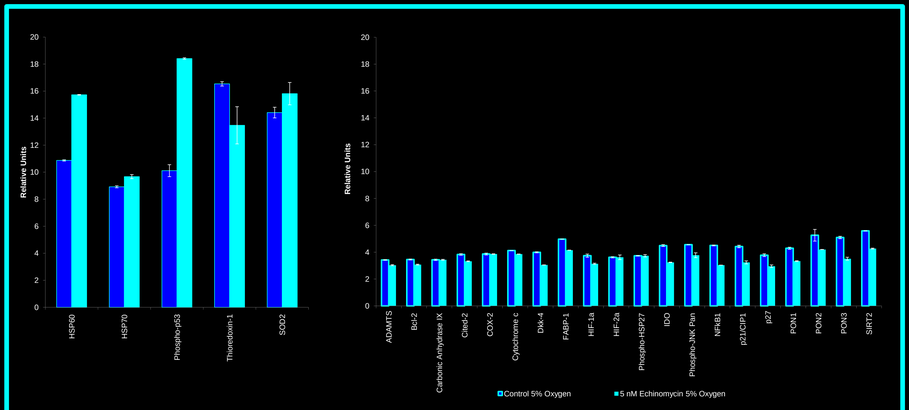

Figure 5. Human cell stress array.
Proteins harvested from both untreated S2VP10 control cells placed in hypoxic conditions and S2VP10 cells treated with 5 nM echinomycin for 24 hours in hypoxic conditions were incubated on nitrocellulose membranes containing binding sites for twenty-six cell stress related proteins. Relative levels of proteins were compared to standard reference spots on the membranes.

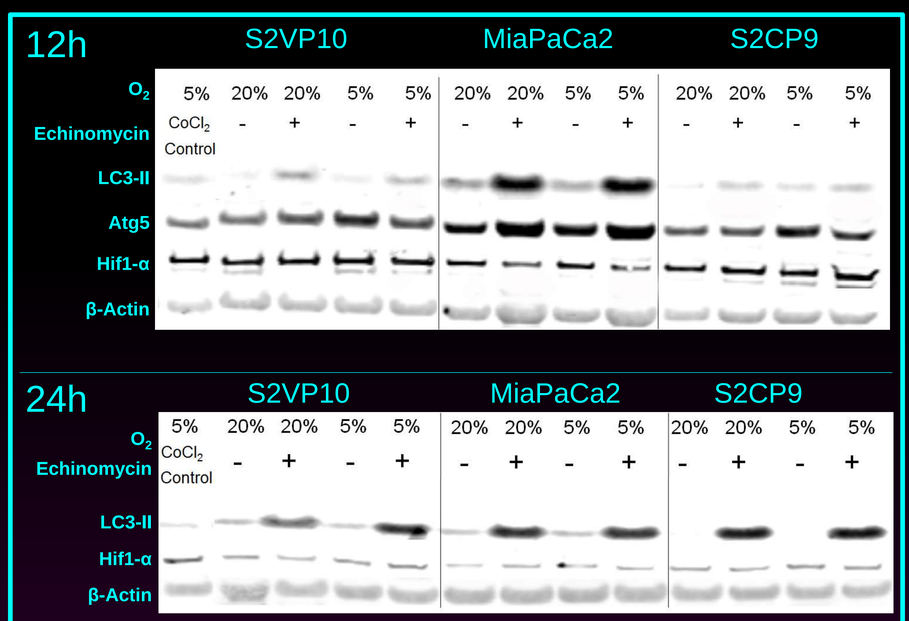

Figure 6. Western blot analysis of S2VP10, MiaPaCa2, and S2CP9 proteins from untreated control cells or cells treated with 10 nM echinomycin for 12 and 24 hours.
Treated cells showed a greater increase in the autophagy marker proteins LC3-II in comparison to untreated control cells. Oxygen level did not alter expression of LC3-II. Hif1-α levels were reduced with Echinomycin treatment in MiaPaCa2 cells at 12 h, but not significantly altered at 24h. ATG5 was altered in less aggressive MiaPaCa2 cells at 12 h in accordance with the increase in LC3-II.

CONCLUSIONS

- Echinomycin treatment of pancreatic adenocarcinoma cells resulted in microscopic vesicles.
- Echinomycin treatment decreases pancreatic adenocarcinoma cell viability through inhibition of autophagy, as demonstrated by LC3-II protein analysis, rather than through apoptosis.
- Echinomycin treatment causes a greater decrease in cell viability in hypoxic conditions in comparison to normoxic conditions.

Future Directions

- Evaluate in vivo therapeutic efficacy of Echinomycin for pancreatic adenocarcinoma.
- Further evaluate mechanism of action for Echinomycin

ACKNOWLEGEMENTS

This project was supported by (NCI grant R00-CA139050) and the R25 Cancer Education Program at the University of Louisville (NIH/NCI grant R25-CA134283).

Examination of Combined Effects of Well-done meat, and Rapid *N*-acetyltransferase 1 and 2 on Breast Cancer Risk among Participants of the Iowa's Women's Health Study

Christina Hickey[1], David W. Hein[1, 2], Mark A. Doll[1], La Creis R. Kidd[1]

[1]Department of Pharmacology & Toxicology, School of Medicine, University of Louisville (UofL), Louisville, KY.

INTRODUCTION

Meat and Cigarette Derived Pro- carcinogens and Their Role In Breast cancer (BrCa)

- Potent meat- or cigarette-derived pro-carcinogens have been implicated in BrCa development.
  - e.g., polycyclic aromatic hydrocarbons (PAH), heterocyclic amines (HCA) and aromatic amines
- Following metabolic activation, resulting genotoxic species may lead to DNA adduct formation and cause tumors in rat mammary glands.

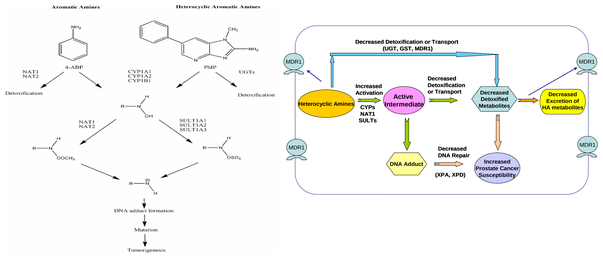

Epidemiological Evidence of the Role of Cooked Meat, Meat Doneness & Variant Carcinogen Metabolism Genes on BrCA

Allele/Genotype	Exposure	OR (95%CI)	Reference
---	Fried/broiled Meat		Zheng et al., 1998
	Fish	4.7 (1.9-12.2)	
	Poultry	16.2 (9.5-27.1)	
	Beef	2.21 (1.30-3.77)	
	Bacon	1.64 (0.92-2.93)	
	Combined Meat	5.1 (1.3-14.2)	
---	Well done meat		Zheng et al., 2009
---	IQ	3.3 (1.8-6.0)	DeStefani et al., 1997
	MeIQx	2.1 (1.3-3.6)	
	PhIP	2.6 (1.4-4.7)	
CYP1A2*F CC	---	2.75 (1.47-5.14)	Sangrajrang et al., 2009
NAT1*11	---	3.9 (1.5-10.5)	Zheng et al., 1999
NAT1*11	Smoking	13.2 (1.5-116.0)	Zheng et al., 1999
NAT2*Slow	---	1.5 (1.2-1.8)	Collishaw et al., 2009
NAT2 Rapid/intermed.	Smoking	5.0 (1.5-16.8)	Dietz et al., 2000
NAT2 Rapid/intermed.	Well done meat	3.3 (1.6-6.8)	Dietz et al., 2000

RESEARCH OBJECTIVE

- We evaluated individual effects as well as complex interactions among three variant carcinogen metabolism genes, tobacco smoking, and preferences towards meats prepared well done as modifiers of breast cancer

HYPOTHESIS

- Individuals who inherited two or more high-risk carcinogen metabolism genes (*CYP1A2*F, NAT1*10/11,* slow *NAT2*5,*) would have an increased risk of developing breast cancer.
  - These effects may be exasperated by exposure to direct or indirect exposure to cigarette or meat-derived carcinogens

CLINICAL RELEVANCE

- Individual susceptibility toward cancer depends on whether a person's genetic makeup interacts with environmental exposures to hazardous chemicals.
- Ultimately, we hope to predict in individuals:
  - with a high likelihood to develop BrCa based on their genetic makeup;
  - who would benefit from preventative intervention strategies.

METHODS

Study Design

- Using a nested case-control study design, we evaluated the independent and joint modifying effects of carcinogen metabolism related SNPs and lifestyle factors in relation to BrCa risk.
- Two hundred seventy-three BrCa cases and 657 disease-free female participants of the Iowa Women's Health Study (IWHS) cohort were used in the current study.

Genetic Analysis

- CYP1A2 and NAT SNPs were detected and evaluated in germ-line DNA using RFLP-PCR and RT-PCR Taqman assays, respectively.

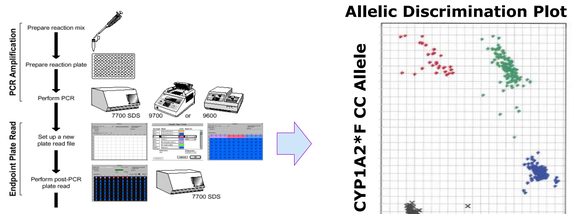

Statistical Analysis

Logistic Regression Modeling

$\text{Logit} = \beta_0 + \beta_{1*}\text{environment}$

$\text{Logit} = \beta_0 + \beta_{1*}\text{gene}_1$

$\text{Logit} = \beta_0 + \beta_1\text{gene} + \beta_2\text{gene}_2 + \beta_3\text{gene}_1{*}\text{gene}_2$

$\text{Logit} = \beta_0 + \beta_1\text{gene} + \beta_2\text{environment} + \beta_3\text{gene*environment}$

Figure 1. Multi-factor Dimensionality Reduction (MDR)

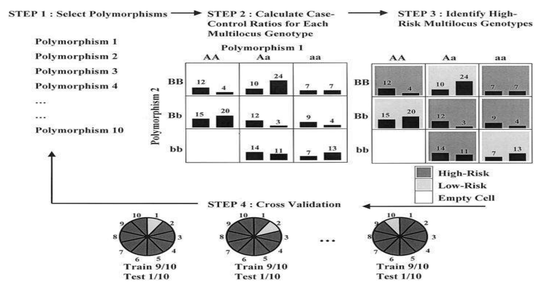

Figure 2. Entropy Graph

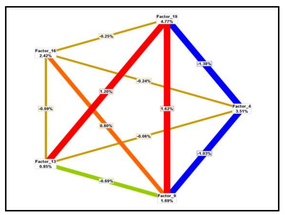

Red, gold, green, and blue lines indicate strong synergy, moderate synergy, Neutral, moderate redundancy and strong redundancy, respectively.

Table 1. Demographic and lifestyle Characteristics among Participants of the IWHS

Demographic and major risk factors	Cases (n = 273)	Controls (n = 657)	P-value (P-trend)	P-trend
Age, median (range)	61 (55-69)	61 (55-70)	0.120	
WHR, median (range)	0.83 (0.65-2.05)	0.82 (0.55-1.64)	0.028	
Family History, n (%)				
No	226 (82.8)	589 (89.6)	0.004	
Yes	47 (17.2)	68 (10.4)		
BMI†			0.088	0.032
Underweight or Normal, n (%)	97 (35.5)	271 (41.2)		
Overweight, n (%)	105 (38.5)	255 (38.8)	0.398	
Obese, n (%)	71 (26.0)	131 (19.9)	0.028	
Age at menarche, n (%)			0.381	
> 13 years of age	70 (25.6)	187 (28.5)		
≤ 13 years of age	203 (74.4)	470 (71.5)		
Age of last menstruation, n (%)			0.824	
≤ 50 yrs	170 (62.3)	404 (61.5)		
>50 yrs	103 (37.7)	253 (38.5)		
# of live births, n (%)			0.152	
< 3	166 (60.8)	432 (65.8)		
≥ 3	107 (39.2)	225 (34.2)		
Age at 1st live birth, n (%)			0.697	
<25 yrs	185 (72.6)	436 (71.2)		
≥25 yrs	70 (27.4)	176 (28.8)		
No live births	18 (6.6)	45 (6.7)		
Alcohol intake, n (%)			0.550	
< 30 g/day	264 (96.7)	640 (97.4)		
≥ 30 g/day	9 (3.3)	17 (2.6)		
Smoking Status			0.405	
Never smoker	179 (66.5)	448 (69.3)		
Ever smoker	90 (33.5)	198 (30.7)		
Missing	4 (1.5)	11 (1.7)		
Red Meat Consumption, n (%)			0.181	0.321
1st quartile	63 (23.1)	170 (25.9)		
2nd quartile	62 (22.7)	170 (25.9)	0.939	
3rd quartile	67 (24.5)	166 (25.2)	0.680	
4th quartile	81 (29.7)	151 (23.0)	0.067	
Doneness Preference, n (%)			0.0008	0.003
Rare or medium	60 (24.6)	224 (37.9)		
Well done	71 (29.1)	155 (26.2)	0.0086	
Very well done	113 (46.3)	212 (35.9)	0.0002	
Well and very well done	184 (75.4)	367 (62.1)	0.0002	

Table 2. Relationship between Carcinogen Metabolism Genes and Breast Cancer Risk among WHS Participants.

Genetic Variants	Cases (n=273)	Controls (n = 657)	$OR_{adj}$$	p-value
CYP1A2*F genotypes (phenotypes)				0.368
CC (low inducibility)	10 (5.9)	37 (9.4)	1.00 (referent)	
AC (intermediate inducibility)	70 (41.4)	151 (38.2)	1.52 (0.70-3.27)	0.161
AA (high inducibility)	89 (52.7)	207 (52.4)	1.49 (0.70-3.17)	0.220
AA vs. (CC/AC)	89 (52.7)	207 (52.4)	1.05 (0.73-1.52)	0.955
Missing	104 (38.0)	262 (39.9)		
NAT1*alleles				0.045
*3/*4 alleles	107 (53.5)	300 (64.1)	1.00 (referent)	
*10 allele(s)	67 (33.5)	121 (25.9)	1.54 (1.08-2.18)	0.020
*11 allele(s)	13 (6.5)	7 (3.6)	2.26 (1.06-4.80)	0.053
*14, *15, *17 or *22 allele(s)	13 (6.5)	30 (6.4)	1.26 (0.64-2.50)	0.635
Missing	73 (26.7)	189 (28.8)		
NAT2 Phenotype				
Slow or very slow acetylators	109 (53.7)	282 (56.4)	1.00 (referent)	
Intermediate acetylators	81 (39.9)	187 (37.4)	1.15 (0.81-1.64)	0.514
Rapid acetylators	13 (6.4)	31 (6.2)	1.00 (0.50-2.01)	0.815
Intermediate and rapid acetylators	94 (46.3)	218 (43.6)	1.13 (0.81-1.58)	0.513
Missing	70 (25.6)	157 (23.9)		

Table 3. Joint Modifying Effects among Variant Carcinogen Metabolism Genes and Well Done Meat in Relation to Breast Cancer Risk among IWHS Participants.

Reference Group	Risk Genotype	Exposure	ORadj (95%CI)
CYP1A2*slow/inter NAT1*3/*4	CYP1A2*slow/inter NAT1*10	---	2.43 (1.42-4.17)
	CYP1A2*slow/inter NAT1*11	---	10.54 (2.74-40.52)
	CYP1A2*rapid NAT1*10		1.91 (1.14-3.19)
	CYP1A2*rapid NAT1*11		2.74 (1.10-6.84)
NAT2*slow rare/medium meat intake	NAT2*slow	Well / Very Well Done Meat	2.05 (1.15-3.65)
	NAT2*rapid/inter		2.47 (1.37-4.44)
NAT1*3/*4	NAT1*3/4		1.82 (1.10-3.00
	NAT1*10/11 CYP1A2*slow/inter		2.61 (1.52-4.48)
	NAT1*10 CYP1A2*slow/ inter		2.43 (1.42-4.17)
	NAT1*11 CYP1A2*slow/ inter		10.54 (2.74-40.52)
	NAT1*14,15,17,22		1.91 (1.14-3.19)

Table 4. Evaluation of Main Effects and Interactions among Carcinogen Metabolism SNPs as Predictors of BrCa using Entropy Based MDR

Best Model	CVC	ATA	MDRpt P-value
One Factor doneness	10/10	0.559	0.035
Two Factor Doneness NAT1_10	8/10	0.556	0.048
Three Factor Doneness, NAT1_10, CYP1A2	9/10	0.582	0.002
Four Factor NAT2Phen, doneness, NAT1_10, CYP1A2	10/10	0.590	0.002

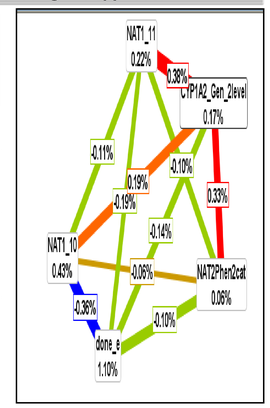

Abbreviations: CVC = Cross validation consistency;
ATA = average testing accuracy; MDRpt P-value = MDR permutation testing p-value

CONCLUSIONS

- Consumption of well/very well done meat was related to a 1.8-1.9 fold increase in BrCa risk using LR modeling.
- Inheritance of at least one NAT1*10 or NAT1*11 alleles was linked to a 1.5-2.3 fold increase in BrCa risk.
- In an exploratory analysis, complex interactions among 3 carcinogen metabolism genes (CYP1A2, NAT1*10, and NAT2) combined with consumption of meats prepared well done may influence BrCa risk.

FUTURE DIRECTIONS

- Upcoming studies evaluate complex interactions among biotransformation genes and environmental exposures and their joint effects in predicting individual predisposition toward BrCa Risk
  - This will require a larger sample size and sophisticated visualization tools to evaluate complex interactions.
- Our approach may be used to identify women who would benefit from intervention strategies based on their genetic and lifestyle preferences.

ACKNOWLEDGEMENTS

- NCI R25 Cancer Education Grant to D.W. Hein (CA134283); Our Highest Potential" in Cancer Research Endowment to LRK.

UBQLN1 regulates IGF1R signaling pathway

Gretchen E. Holz[1], Levi J. Beverly, Ph.D.[2]
R25 Trainee[1] and Department of Medicine, James Graham Brown Cancer Center[2]
University of Louisville School of Medicine

Abstract

Many growth factor receptors are known to play key roles in the development of cancer, so it is critical to understand the components and mechanisms involved in their signaling pathways. However, current knowledge on these details is limited. The type I insulin-like growth factor receptor (IGF1R) stimulates a signaling pathway that leads to cell growth and proliferation in normal cells, and the IGF1R pathway is often deregulated in human lung adenocarcinoma. Details regarding early players and events in this pathway are incomplete. Our previous data show that Ubiquilin1 (UBQLN1), a cytosolic protein known to be involved in a variety of homeostatic cellular processes, like regulation of protein degradation and receptor trafficking, is upregulated in non-small cell lung cancer (NSCLC) cells. In addition, upregulation of UBQLN1 proves to be predictive of long-term outcome of patients. Herein, we demonstrate a novel protein interaction between IGF1R and UBQLN1, which thus implies UBQLN1 plays a role in regulating the IGF1R pathway. This preliminary research may lead us to a more complete understanding of IGF1R's endocytic pathway, including the mechanisms and components necessary to continue the signal and/or recycle the receptor. Ultimately, these details are of great importance as more than 100 clinical trials have been conducted to assess the potential of inhibiting IGF1R signaling as a cancer therapy. The trials have varied in success suggesting a critical need to target different and more specific avenues for more consistent therapeutic results.

Questions

- Does UBQLN1 affect levels of IGF1R and/or E-SYT2? Does IGF1R affect levels of UBQLN1 and/or E-SYT2? Does E-SYT2 affect levels of UBQLN1 and/or IGF1R?
- Do UBQLN1, IGF1R, and E-SYT2 interact in cells?
- Are there changes in the level of phosphorylated IGF1R (P-IGF1R) upon over-expression of UBQLN1? E-SYT2?

Results

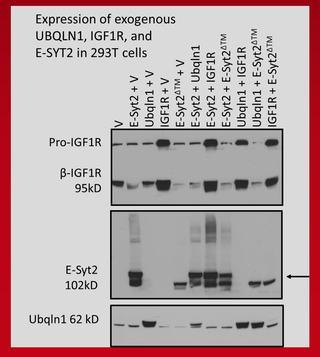

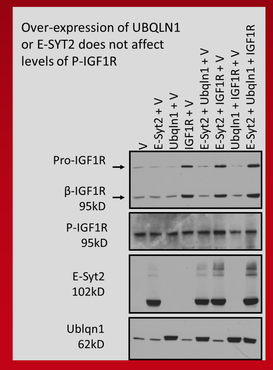

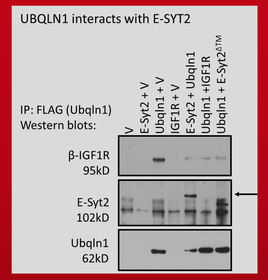

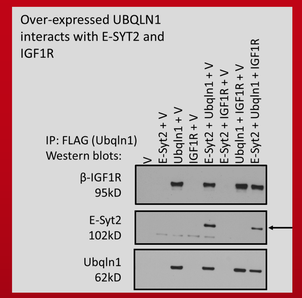

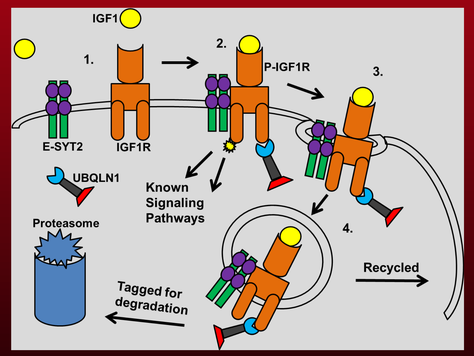

1.) IGF1R and E-SYT2 are transmembrane proteins. Insulin-like growth factor 1 (IGF1) is a ligand that binds and activates IGF1R. 2.) IGF1 binds IGF1R, which is activated at its tyrosine kinase domain, creating a signal cascade through the cell that leads to cell proliferation. This activation of IGF1R may also be a signal for E-SYT2 and UBQLN1 to bind or associate with the receptor. 3.) The association of these proteins with IGF1R may then facilitate its endocytosis. Specifically, E-SYT2 may need to bind IGF1R in order for endocytosis to occur. E-SYT2's specific function is unknown, but studies have shown its involvement in membrane trafficking, particularly endocytosis of growth receptors. We are in the early stages of showing data that E-SYT2 has a specific relationship to IGF1R. 4.) The specific route of IGF1R's endocytic pathway may be determined by bound UBQLN1, which may work as a tag or marker for intracellular IGF1R. UBQLN1 may tag IGF1R as a protein to be degraded, so IGF1R will be routed to the proteasome. UBQLN1 may be a tag that sends IGF1R back to the membrane to continue its function.

Conclusions

This project focused on the novel relationship between UBQLN1 and IGF1R and an emerging interest in E-SYT2's interaction with UBQLN 1 and IGF1R. From the data we gathered, we concluded that UBQLN1 does interact with both IGF1R and E-SYT2. The data do not reveal noteworthy changes in the phenotypes of UBQLN1, IGF1R, or E-SYT2 in experiments involving over-expression. We also did not see definitive results in how over-expression of UBQLN1 and E-SYT2 impacts the level of activated IGF1R. Thus, we did find positive and negative results to our initial experimental questions, suggesting that more research is required to answer the key questions regarding the details behind the interactions between UBQLN1, IGF1R, and E-SYT2.

Future Directions

- What results do we get if we over-express the same proteins, serum starve 293T cells, and then treat with differing concentrations of IGF1R's primary ligand, IGF1?
- Will the immunoprecipitation of E-SYT2 be more successful with a different type of lysis buffer?
- Can these experiments be duplicated with similar results in other adenocarcinoma cell lines—A549, PC9?
- What results do we get if we do these experiments with knock-down of UBQLN1, IGF1R, and E-SYT2?
- Fluorescent labeling of IGF1 and/or IGF1R to analyze intracellular movements and pathways
- Using flow cytometry in concert with these experiments to analyze cell-surface exposed IGF1R

Acknowledgements

Research supported by a grant from Kosair Pediatric Cancer Program and NCI R25 grant support of University of Louisville Cancer Education Program NIH/NCI (R25- CA134283).

Increased Human Arylamine *N*-Acetyltransferase 1 Inhibition and Breast Cancer Cell Progression by Curcumin and/or Resveratrol in Combination with Compound 10

Nicole M. Jackson[1,3], Carmine S. Leggett, Ph.D.[1,3], Mark A. Doll, M.S.[1,3], J. Christopher States, Ph.D.[1,3,4], and David W. Hein, Ph.D.[1,3,4]

Department of Pharmacology and Toxicology[1], Department of Medicine [2], James Graham Brown Cancer Center [3] and Center for Environmental Genomics and Integrative Biology[4]

University of Louisville School of Medicine

Louisville, KY 40202

Abstract

Human arylamine *N*-acetyltransferase 1 (NAT1) plays an important role in metabolizing environmental carcinogens and cancer progression. Studies completed in our laboratory have determined that a small molecule inhibitor, Compound 10, inhibits NAT1 activity, and causes a decrease in cell invasion and cell proliferation in human breast adenocarcinoma cells. In the present study, we hypothesize that Compound 10 is a more effective and/or potent NAT1 inhibitor in combination with chemopreventive agents such as curcumin or resveratrol. We also postulate that the inhibition of human NAT1 by Compound 10 in combination with these chemopreventive agents will further decrease NAT1 metabolism, cell invasion, and metastasis in human breast adenocarcinoma cells. In yeast lysate that recombinantly express human NAT1, Compound 10 (0.75 μM) exhibited 77% NAT1 inhibition, whereas Compound 10 in combination with curcumin (100 μM) exhibited 90% inhibition ($p < 0.001$) and in combination with resveratrol exhibited 97% inhibition ($p < 0.001$). Compound 10 also dramatically increased the potency of curcumin and resveratrol as inhibitors of human NAT1 recombinantly expressed in yeast. The IC_{50} for curcumin decreased over 10,000-fold, from 134 to 0.0131 μM in the presence of Compound 10 at its IC_{50} of 0.75 μM. Similarly, the IC_{50} for resveratrol decreased over 700-fold, from 1230 to 1.73 μM in the presence of compound 10 at its IC_{50} of 0.75 μM. In MDA-MB-231 human breast adenocarcinoma cells, Compound 10 exhibited 68% NAT1 inhibition in situ whereas Compound 10 in combination with curcumin exhibited 91% inhibition ($p<0.001$) and Compound 10 in combination with both curcumin and resveratrol exhibited 95% inhibition ($p <0.001$). A combination of 100 μM Compound 10 with 100 μM curcumin slightly but significantly ($p<0.05$) reduced cell invasion compared to treatment with Compound 10 or curcumin alone. Similarly, cell adhesion was reduced significantly more by the combination of Compound 10 and curcumin ($p<0.05$) as well as the combination of Compound 10 and resveratrol ($p<0.05$), compared to Compound 10 alone. In conclusion, Compound 10 was synergistic with other chemopreventative agents in human NAT1 inhibition, cell invasion, and cell adhesion assays. Its usefulness in combination with these agents should be further explored as a cancer treatment option. [Partially supported by the University of Louisville Cancer Education Program (NCI R25-CA134283).]

Introduction

- Human arylamine *N*-Acetyltransferase1 (NAT1) is a phase II metabolizing enzyme that plays an important role in metabolizing environmental carcinogens.
- NAT1 catalyzes *O*-acetylation, which leads to the formation of DNA adducts, and cancer initiation. NAT1 has also been associated with several cancers such as breast, urinary bladder, and lung cancer.
- Studies completed in our laboratory identified a small molecule inhibitor, Compound 10, that decreases NAT1 activity and decreases cell adhesion and cell invasion in human breast adenocarcinoma cells.
- The purpose of this study is to investigate the effects of Compound 10 in combination with chemopreventive agents curcumin and resveratrol on NAT1 activity, cell invasion, and cell adhesion.

Objective

- To evaluate the effects of chemical inhibition of NAT1 on cell invasion and cell adhesion in human breast adenocarcinoma cells lines.

Hypotheses

- Inhibition of human NAT1 by Compound 10 in combination with curcumin or resveratrol will decrease NAT1 activity at a greater capacity than Compound 10 alone.
- Inhibition of human NAT1 by Compound 10 in combination with curcumin or resveratrol will decrease cell invasion in human breast adenocarcinoma cells.

Results

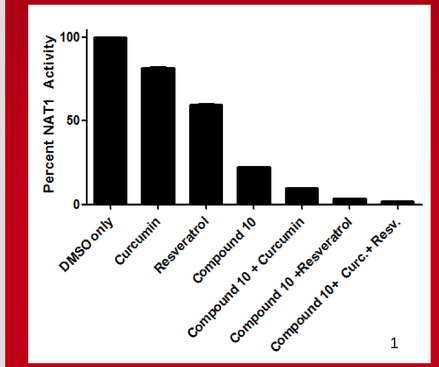

Figure 1. *In vitro* NAT1 activity was determined by using 100 μM acetyl coenzyme A and 300 μM para-aminobenzoic acid (PABA) with 50 μM curcumin, 50 μM resveratrol, 50 μM Compound 10, or various combinations of the three agents in lysates of yeast which express recombinant human NAT1.

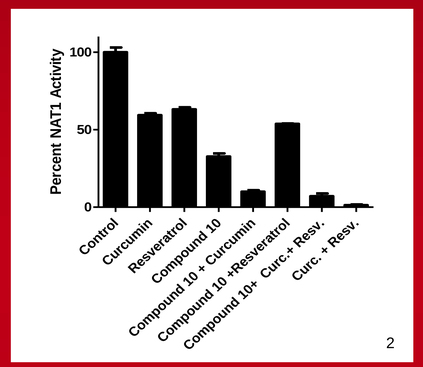

Figure 2. *In situ* NAT1 activity was determined in MDA-MB-231 human breast adenocarcinoma cells, which endogenously express human NAT1. Cells were treated with Dulbecco's Modified Eagle Medium (DMEM) supplemented with 100 μM total reaction concentrations of PABA with curcumin, resveratrol, Compound 10, or various combinations of Compound 10 with curcumin and resveratrol.

Compounds	IC_{50}	IC_{50} with Compound 10
Compound 10	0.75 μM	N/A
Curcumin	134 μM	0.0131μM
Resveratrol	1230 μM	1.73 μM

3

Figure 3. IC_{50} values of curcumin and resveratrol (separately, and in combination with 0.75 μM Compound 10) were determined using 100 μM of acetyl coenzyme A and 300 μM of PABA with various concentrations of curcumin or resveratrol (0-1000 μM) in yeast lysate.

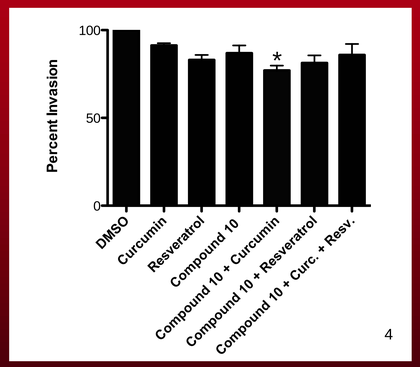

Figure 4. Inhibition of cell invasion by Compound 10, curcumin, and resveratrol in MDA-MB-231 cells. Cells (300,000) were seeded and allowed to invade towards culture media containing 10% FBS for 24 h in the presence of various combinations of the selected agents (100 μM each). Cells on the bottom of the polycarbonate membrane were stained, extracted, and the absorbance was quantified at 560 nm. Cell invasion was plotted as the percentage of untreated cells (control). Each point represents the mean ± SEM for 3 experiments. Cells were allowed to polycarbonate membrane were extracted, stained, and quantified using a 96 well plate reader at 560 nm. Each data set was compared to the DMSO control in order to determine percent invasion. Compound 10 in combination with curcumin ($p<0.05$), were the only data which showed statistical difference in comparison to DMSO.

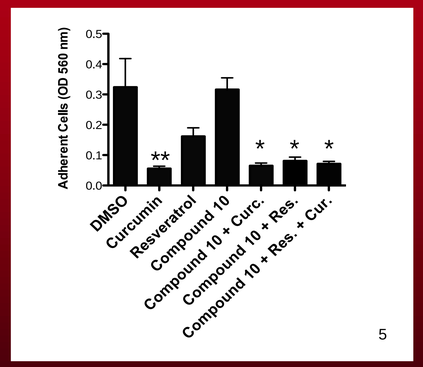

Figure 5. MDA-MB-231 cells were treated with 100 μM of each drug and/or drug combination with Compound 10 for a period of 60 minutes. Adherent cells were extracted, stained, and quantified using a 96-Well plate reader at 560 nm. Curcumin ($p<0.01$), Compound 10 with curcumin ($p<0.05$), Compound 10 with resveratrol ($p<0.05$), and Compound 10 with both curcumin and resveratrol ($p<0.05$) were the data within this assay which showed statistical difference in comparison to DMSO.

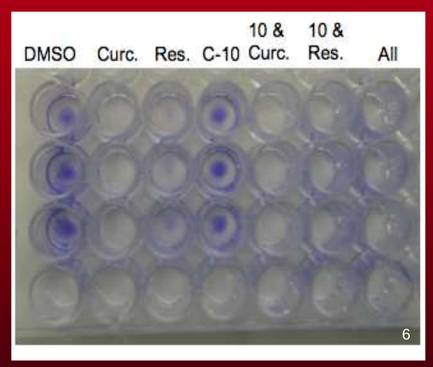

Figure 6. Representative photograph of the cell staining step within the 48-Well cell invasion assay procedure. Serum starved cells were allowed to attach to a Collagen-1 coated 48-Well cell adhesion plate for 60 minutes at 150,000 cells per well. Adherent cells were stained prior to quantification of the absorbance at 560 nm.

Methods

- *In vitro* NAT1 activity assays were performed using lysates of yeast which express recombinant human NAT1. The acetylated product was quantified using High Performance Liquid Chromatography.
- MDA-MB-231 human breast adenocarcinoma cancer cells were cultured in Dulbecco's Modified Eagle Medium (DMEM), supplemented with 10% Fetal Bovine Serum (FBS).
- *In situ* NAT1 activity assays were performed using MDA-MB-231 human breast adenocarcinoma cells which endogenously express human NAT1. The activity was then quantified using High Performance Liquid Chromatography.
- A 24-Well Cell Invasion Assay was obtained from Cell Biolabs, Inc. Cells which invaded through the polycarbonate basement chamber (invasive cells) were washed, stained and quantified using a 96-Well plate reader at 560 nm.
- A 48-Well Cell Invasion Assay was obtained from Cell Biolabs, Inc. Cells which adhered to the bovine collagen plates were washed, stained and quantified using a 96-Well plate reader at 560 nm.

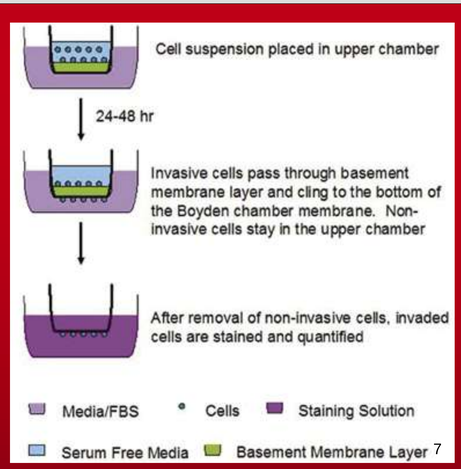

Figure 7 Representative photograph describing the procedure of the 24-Well cell invasion assay (Photograph obtained from www.cellbiolabs.com). 300,000 cells were seeded in serum deprived of fetal bovine serum (FBS). The cells were then allowed to invade through a polycarbonate membrane into serum containing FBS. Invasive cells were extracted and stained. The absorbance of these cells was then quantified using a 96-Well plate reader at 560 nm.

Conclusions

- Compound 10 in combination with curcumin is a more potent human NAT1 inhibitor than Compound 10 alone.
- Compound 10 was synergistic with both curcumin and resveratrol in human NAT1 inhibition, in both cell invasion assays.
- Compound 10 in combination with curcumin and resveratrol appears to be an attractive drug combination for cancer therapeutics, and should be further investigated.

Acknowledgements

Partially supported by the University of Louisville Cancer Education Program (NCI R25-CA134283).

Developing Computational Tools for Molecular Comparison and Metabolic Placement of Detectable Uncharacterized Metabolites

UNIVERSITY OF LOUISVILLE®

Joshua M. Mitchell and Hunter N.B. Moseley
Department of Chemistry, University of Louisville, KY USA

Center for Regulatory and Environmental REAM Analytical Metabolomics

♦ Abstract

Metabolism is the set of chemical reactions that occur in living systems that make life possible. The majority of these chemical reactions are catalyzed by protein enzymes which interconvert a vast network of organic molecules (metabolites) into forms needed for cells to live and grow. Detection and identification of these metabolites is key to modeling and understanding these vast metabolic networks. Advances in metabolomics, especially in ultra-high resolution mass spectrometry enable the rapid analysis of many thousands of peaks (observables) representing a few thousand metabolites. However, a key barrier to meaningful interpretation of this mass spectrometry (MS) data is the identification of detectable but unknown metabolites from mass spectrometry. Recent development of chemoselective (CS) probes that tag metabolite functional groups not only boosts the speed and accuracy of metabolite detection, but provides new computational avenues for metabolite identification. We are developing algorithms that combine this additional functional group information with molecular formulas to improve metabolite identification. These algorithms enable combined molecular formula and functional group searches of metabolite and organic compound databases via fast detection of functional groups in molecular compound databases. This ability to identify the functional groups and the molecular formulas of query structures lends itself to the identification of compounds via chemoselective tagging, adduct formation, and detection in ultra-high resolution mass spectrometers like the Fourier transform-ion cyclotron resonance-MS (FT-ICR-MS). By comparing the molecular formulas and the functional group substructures of query compounds to entries in the Human Metabolome Database (HMDB), KEGG Compound, and other databases, similar molecules can be detected when perfect matches are not found. Correlation in similar compounds can generate hypotheses for where newly discovered metabolites fit within metabolic networks of interest like human metabolism. These efforts will aid in filling out our incomplete picture of human metabolic networks. Furthermore, systematic analysis of molecular compound databases will: i) identify the distribution of isomers across these databases, ii) determine the limitations of these combined analytical and computational approaches; and iii) and provide clear direction for improvement of these methods.

♦ Introduction

Metabolites are the small intermediates and products of metabolism. They range in complexity from very small bioorganic compounds consisting of a handful of atoms to more complex structures consisting of a few hundred atoms. The study of metabolites and metabolism sheds light on the study of life as a whole and has important implications in many areas of biological and biomedical research. However, the study of these complex processes requires the development of sophisticated databases and tools to access them. Several metabolic databases aggregate scientific knowledge of cellular metabolism and specifically of known metabolites, including HMDB and KEGG Ligand. In particular, the HMDB contains comprehensive information on human metabolites, including the structure of over 7900 discovered human metabolites as well as ionization information, stereochemical information, atom and bond counts and the atoms present in each compound, excluding hydrogens in MOL file format.

We are developing tools that can detect similarity between a query molecule and database compounds, by creating an abstraction of each molecule as a graph, wherein the atoms become nodes and the bonds vertices. As graphs, the problem of detecting similarity between two compounds becomes analogous to the problem of finding the largest region that the two graphs have in common. Fortunately, this is a well documented problem in graph theory called the maximum common subgraph isomorphism (MCSI) problem and a variety of algorithms are available for finding solutions to this problem, such as the Ullmann Algorithm [3]. To use these algorithms, we must represent graphs for compounds in a numerical form such as an adjacency matrix (Figure 1).

Figure 1: Pictorial representation of Acetone, Acetone's MOL File, a graphical representation, the adjacency matrix for acetone.

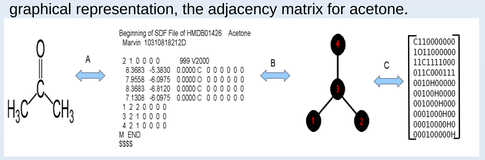

With adjacency matrices for both a query and target molecule, the Ullmann algorithm generates a series of matrices representing each possible mapping of each atom in the query compound to each atom in the database entry. Through node coloring, we can reduce the number of irrelevant mappings (i.e. atoms of different element types will not be mapped to one another). These mapping matrices are then processed, the isomorphisms identified, and the amount of similarity quantified through the Tanimoto Coefficient [4]. Since the similarity scores are indicative of their relative position to one another in the metabolic network, high scores can provide hypotheses for where query compounds belong in a metabolic network. Furthermore, the identification of functional groups in query and database compounds can enhance the similarity scoring of related metabolites. Thus, the use of adduct and derivative formation in the identification of new metabolites can help in the analysis of detected metabolites from Fourier transform ion cyclotron resonance mass spectrometry data (FT-ICR-MS). For example, a database can be searched to find all compounds matching a specific formula that contain a given functional group.

With our metabolite comparison tools, we can perform a variety of analyses on the HMDB and other related databases. For example, i) how many compounds in a given database are isomers of one another; ii) how many compounds are shared between databases by name, molecular formula, bonded structure; and iii) how many shared compounds are isomers in across databases.

♦ Materials and Methods

♦ Overview

Project development is divided into two parts (Figure 2):

1. Development of database access tools for HMDB and KEGG Compound. This includes tools that convert different metabolite databases into a common MOL file format and parsers that convert this common format into an internal representation.
2. Development of MCSI query and comparison tools via adaptation of Ullmann's algorithm combined with a Tanimoto coefficient formalism (Figure 2).

Figure 2: Flow Chart Representation of the MCSI Query Program.

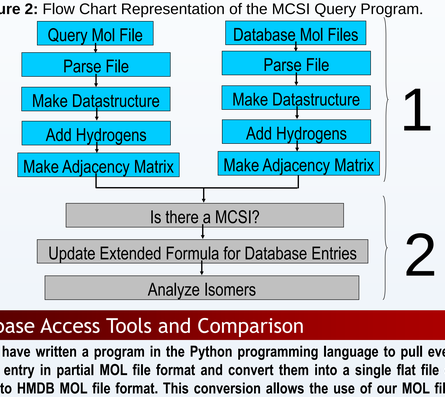

♦ Database Access Tools and Comparison

We have written a program in the Python programming language to pull every KEGG Compound entry in partial MOL file format and convert them into a single flat file of entries analogous to HMDB MOL file format. This conversion allows the use of our MOL file parsing methods (written in Perl programming language) which convert MOL file entries into an internal representation, add missing hydrogens, and create an adjacency matrix representation (Figure 1).

To test our MOL file parsing methods and KEGG Compound database access tools, we performed an initial analysis and comparison of two metabolite databases, HMDB and KEGG Ligand. We wrote a Perl program which performs this comparison in the following steps:

i. Parse both databases from their MOL formatted flat files.
ii. Calculate molecular formulas for each entry.
iii. Create an index of entries for each database based on compound name.
iv. Create an index of entries for each database based on molecular formula.
v. Identify multiple entries with the same molecular formula (isomers) in each database.
vi. Compare entries between databases based on compound name.
   - Identify pairs of entries with different molecular formulas and calculate an average Tanimoto coefficient across the differences.

$$\tau = \frac{(N_{ab})}{(N_a + N_b - N_{ab})}$$

where:

N_{ab} - number of shared atoms of the same element.
N_a , N_b - number of atoms in each database entry.

vii. Compare entries between databases based on molecular formulas.
   - Identify which pairs of entries are isomers in both databases.

Results are shown in Figures 5, 6, and 7.

♦ Results

Figure 4: Database Comparison by Compound

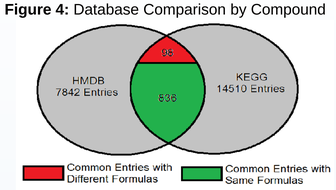

Above are comparisons of the HMDB and KEGG Ligand databases. Of the 7842 entries in the HMDB, 934 matched entries in KEGG by compound name. 836 of the matches had the same formulas, 98 did not. The 98 that did not match had an average Tanimoto coefficient of 0.802.

Figure 5: Database Comparison by Formula

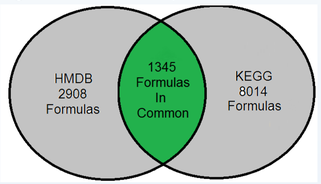

A similar comparison using molecular formula was performed. Between the two databases, there were 1345 molecular formulas in common. Thus, the two databases really do not have that many "metabolites" in common.

Figure 6: Isomer Distribution of Shared Isomers

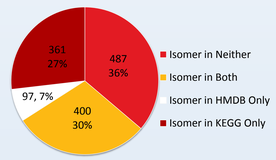

Once these common formulas were identified, each was compared against both databases to determine if the formula was an isomer in neither, both or either database. Of the 1345 formulas, 36% were isomers in neither, 30% were isomers in both, 7% were isomers in the HMDB only, and 27% were isomers in KEGG only.

Figure 7: Isomer Content of Databases by Formula

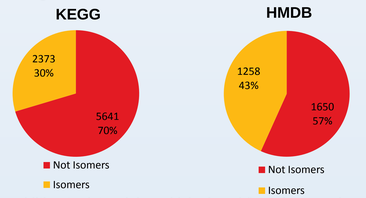

In addition to determining which shared formulas were isomers, each formula in each database was checked to see if it was an isomer within the database. Of the 8014 formulas in KEGG, 2373 or 30% of them were isomers in the database. Of the 2908 formulas in the HMDB, 1258 or 43% of them were isomers.

Figure 8: Stereoisomer Composition of KEGG

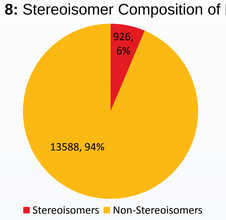

In addition to determining which formulas were isomers in both compounds, the isomeric compounds in KEGG were analyzed to determine which isomers were stereoisomers of at least another compound in the database. Of 14514 compounds in KEGG, 6% or 926 compounds were stereoisomers of at least one other compound. Only one stereisomer was used in the next analysis.

Figure 9: %Compounds in KEGG with specified Functional Group

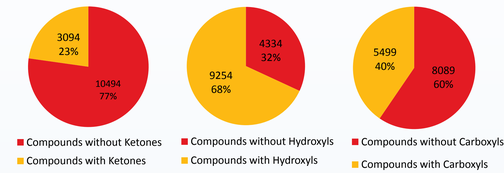

Additionally, the extended formula for each compound in KEGG was determined using the functional groups for which adducts can be readily formed. Using these extended formulas, the number of compounds containing a given functional group was determined.

Figure 10: %Compounds Detectable with MS and Specified Adducts

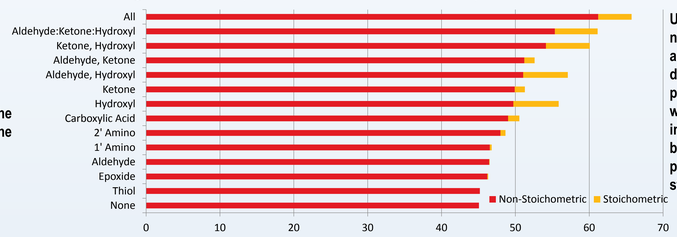

Using these extended formulas, the number of compounds detectable by MS and adduct formation together was determined as well. One analysis was performed assuming adduct formation was stoichometric, that the number of instances of the functional groups could be determined, another analysis performed assuming they were not stoichometric.

♦ Substructure Comparison and Scoring

Given the large number of structural and stereisomers in the metabolome, mass spectrometry alone would be unable to identify these compounds. However, these isomers may differ in their composition of specific functional groups, allowing a combination of mass spectrometry and functional group adduct and derivation formation to identify them. In this approach, the molecular formula for a given metabolite is determined by the ultra-high accurate m/z ratio in FT-ICR-MS, and specific functional groups are determined by the presense of specific adducts or derivatives. To the molecular formula, the present functional groups are appended to produce the 'extended formula' of a compound. This 'extended formula' is used to search for exact or similar matches in a database.

For this approach to succeed, the extended formula for each compound in the reference database must be determined. Given a database compound's MOL file and a functional group's MOL file, the program first adds hydrogens to the database entry as per bonding and charge rules. Then for both MOL files, the program generates their adjacency matrices and a mapping matrix which represents which atoms in the functional group could be mapped to atoms in the database compound. This matrix is then enumerated and each enumeration is checked for legitimate mappings. If a correct mapping is found and includes all the functional group atoms, the functional group is present in the compound. For efficiency, incorrect mappings are used to short-circuit the enumeration process. Enumeration continues until all resulting mappings are either incorrect or correct and all instances of that functional group have been identified. Once identified, the name of the functional group and the number of instances present are appended to the molecular formula.

Figure 3: Determining the Extended Formula for Acetone

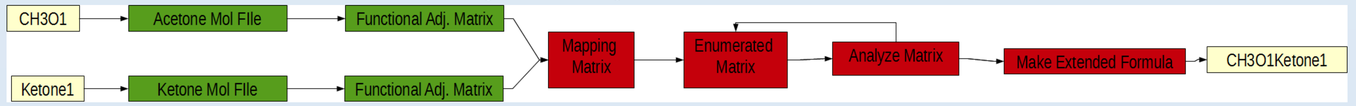

♦ Conclusion

- We have developed methods to parse a MOL file into an internal graph representation which can then be used by our algorithm to identify functional groups within the compound. This data can then be used to determine an extended molecular formula of each compound.
- We can use extended molecular formulas derived from ultra-high accurate mass spectrometry data to identify a greater percentage of compounds than with just a molecular formula. Our analysis of the KEGG database with this method shows that the percentage of MS identifiable compounds increases from 45% to 60% with the use of non-stoichometric adduct formation. Stoichometric adduct formation only offers an additional 5% increase in detectable compounds.
- 30% of the formulas in KEGG and 43% of the isomers in the HMDB have isomers and the stereoisomer content of KEGG was determined to be 6%. The high content of isomers in each database indicates that methods such as adduct and derivative formation will be necessary to identify compounds without tandem mass spectrometry. The low stereoisomer content also implies that there will only be a small number of compounds that cannot be resolved by this approach.

♦ Future Directions

- Perform the same stereoisomer and extended formula analysis on the HMDB and other databases to analyze the effectiveness of adduct formation for identifying metabolites by mass spectrometry.
- Develop tools that can look up compounds by their extended formulas for identification and in cases where identification fails, provide plausible hypotheses as to where the metabolite occurs in metabolism.
- Use subgraph similarity between detected compounds and database compounds to improve the accuracy of these hypotheses. Once these tools are developed, systematically test the accuracy of this hypotheses generation approach.

♦ References

1. *Metabolism Definition* [http://www.medterms.com/script/main/art.asp?articlekey=4359].
2. *Human Metabolome Database* http://www.hmdb.ca/ .
3. Ullmann et al. *An Algorithm for Subgraph Isomorphism, Journal of the Association for Computing Machinery, Vol 23, No 1,* (January 1976).
4. Dogra, Shaillay K., "Script for computing Tanimoto coefficient" from QSARWorld – free online resource for QSAR modeling. http://www.qsarworld.com/virtual-workshop.php,.
5. KEGG Ligand - http://www.genome.jp/kegg/ligand.html

Candidate Drugs Target the APC/C to Induce Mitotic Arrest in Ovarian Cancer

Douglas J. Saforo[1], Brian C. Sils[1], B. Frazier Taylor[2], John O. Trent[3], and J. Christopher States[1]
[1]Pharmacology and Toxicology and [3]Medicine, University of Louisville School of Medicine;
[2]Therapeutic Radiology, Yale School of Medicine

Abstract

Taxanes are a class of chemotherapeutic drug that act to disrupt microtubule function and cause mitotic arrest and cell death. These drugs are commonly used for cancer treatment, however their effectiveness is dependent on the presence of a functioning spindle assembly checkpoint (SAC). As a result, it is possible for cancer cells to become resistant to microtubule disrupting drugs by inactivating the SAC. The anaphase promoting complex/cyclosome (APC/C) is an E3 ubiquitin ligase that acts as the master regulator of cell cycle progression. Inhibition of the APC/C should result in disruption of the cell cycle, resulting in arrest during mitosis and/or pseudo-G1. Previous *in silico* studies of the APC/C structure have yielded potential compounds that bind to the APC/C subunit ANAPC2. Three of these compounds (#8, 10, 11) were tested on A2780/CP70 and SKOV3 ovarian carcinoma cells and tGM24 telomerase immortalized human fibroblasts. Cell morphology was observed during treatment with the compounds and showed signs of mitotic and apoptotic cells in a dose dependent manner. While all compounds showed the predicted effects, effects were more pronounced with compounds 10 and 11 than compound 8. Mitotic index determinations revealed a significant mitotic delay in both cancer cells and fibroblasts treated with compounds 8, 10, and 11. Compounds 10 and 11 were more potent than compound 8 in inhibition of colony forming ability for all three cell lines. Fibroblasts showed some resistance to compound 8, however fibroblasts exposed to compound 11 showed complete inhibition of cell growth without characteristic morphological signs of apoptosis. All three compounds induced apoptosis in ovarian cancer cells, as indicated by increased caspase 3 activity, but not in fibroblasts. These results indicate that compounds targeting the APC/C can induce mitotic arrest and kill ovarian cancer cells while sparing normal cells. This research was supported by the University of Louisville Cancer Education Program NIH/NCI grant R25-CA134283.

Introduction

Ovarian Cancer

The American Cancer society estimates that Ovarian cancer accounts for more deaths than any other cancer of the female reproductive system. In the United States, it is estimated that 22,280 women will be diagnosed with ovarian cancer and that 15,500 will die from ovarian cancer in 2012. While ovarian cancers that are discovered at an early stage have a high degree of successful treatment, a majority of ovarian cancers remain undetected due to symptoms which are commonly confused with other problems. This delay adds further difficulty to treatment and decreases the likelihood of survival.

Ovarian cancers are commonly treated with surgery and chemotherapeutics including platinum compounds and taxanes. Taxanes act by disrupting the normal mechanism of microtubules during cell division leading to mitotic arrest and apoptosis. Unfortunately, these drugs have a side effect of peripheral neuropathy and their function is dependent upon a functional spindle assembly checkpoint (SAC). Cancer cells that lack a fully functional SAC are thus resistant to such treatment, highlighting a need for new drug treatments that target a similar mechanism during cell division.

Anaphase Promoting Complex

- An E3-Ubiquitin Ligase, responsible for the transfer of ubiquitin molecules to a protein target via an isopeptide bond to a lysine side chain followed by elongation of the ubiquitin chain.
- Composed of eleven subunits and two potential activating proteins.
- Catalytic subunit ANAPC11 (a zinc RING finger protein), Scaffolding subunit ANAPC2 (a cullin-like protein), and Activator proteins CDC20 or CDH1 are responsible for selective enzymatic function.
- Master regulator of mitosis and targets include securin, Cyclin B, Cyclin A, geminin and many others.
- Target protein ubiquitination results in degradation by the 26S proteasome.
- Securin degradation releases separase from securing inhibition and allows it to cleave cohesin. Cohesin acts like a “glue” to hold sister chromatids together.

Hypothesis

If candidate compounds block the binding of subunits of the APC/C and inhibit it, then cancer cells will undergo mitotic arrest and either undergo apoptosis during mitosis or proceed to arrest and undergo apoptosis in early G1.

Results

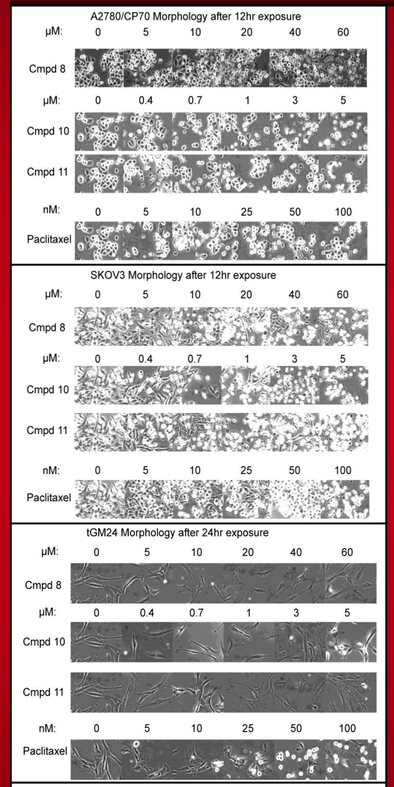

Figure 1. Visual assessment of compound (8, 10, 11) toxicity. Ovarian cancer cells (A2780/CP70 and SKOV3) were plated in a 24-well plate and treated with the indicated concentrations of compounds 8, 10, and 11 over a 24 hour period. Pictures were taken at 6 hour intervals. Diploid fibroblasts (tGM24) were treated with the candidate compounds over a 72 hour period. All cells were treated with paclitaxel as positive control. Round, bright mitotic cells can be observed steadily increasing in number as compound concentration increases. Darker, blebbed apoptotic cells appear at the highest drug concentrations in treated ovarian cancer cells but not in the diploid fibroblasts.

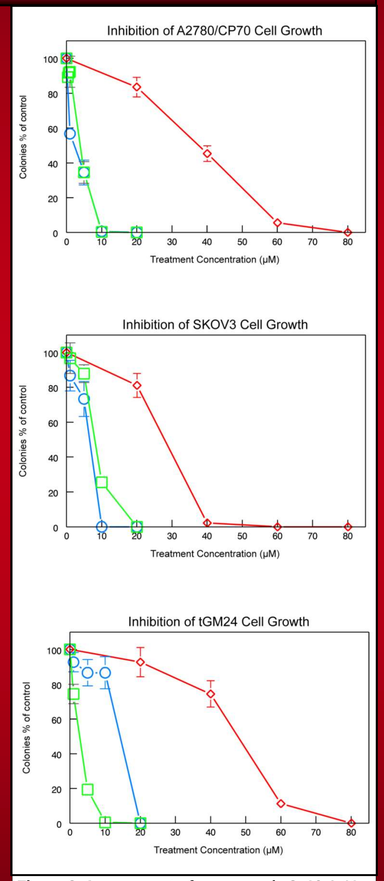

Figure 2. Assessment of compounds 8, 10 & 11 inhibition of cell growth. Ovarian cancer cells (A2780/CP70 and SKOV3) and fibroblasts (tGM24) were plated in a 6-well plate at 100 or 500 cells per well, allowed to attach overnight, and then treated with the indicated concentrations. Colonies were stained and counted after 7 days. Fibroblasts were stained and counted after 14 days. All compounds inhibited cell growth.

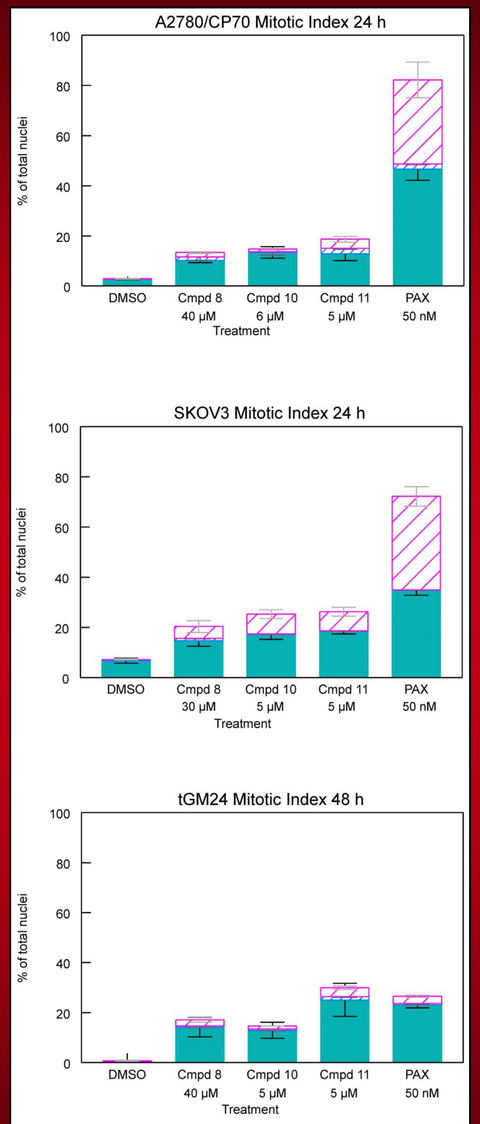

Figure 3. Mitotic index determination. Ovarian cancer cells (A2780/CP70; SKOV3) were treated at the IC50 for compounds 8, 10, and 11 for 24 h. Fibroblasts were treated for 48 h. Paclitaxel was used as a positive control. All compounds induced increases in mitotic index.

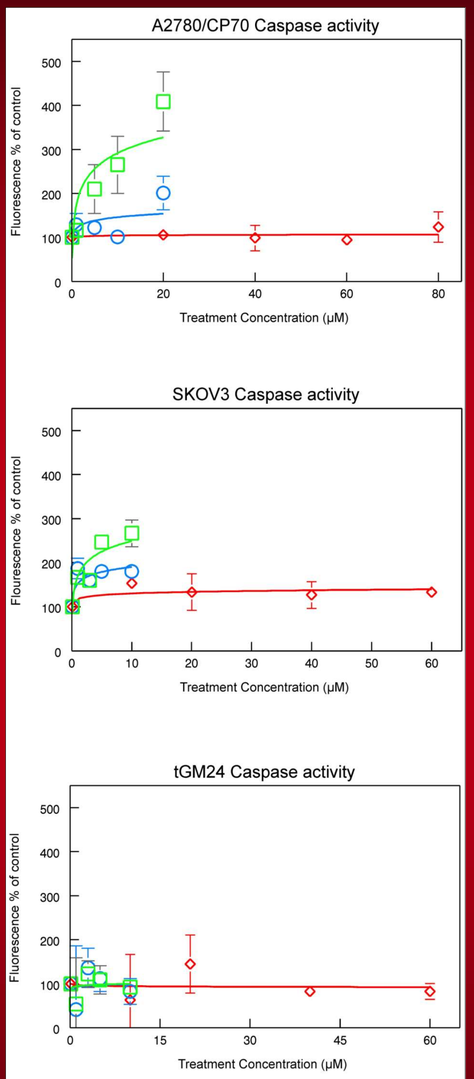

Figure 4. Assessment of caspase 3 activity. Ovarian cancer cells (A2780/CP70 and SKOV3) were plated in a 96-well plate and treated at the indicated concentrations for 24 hours. Fibroblasts (tGM24) were treated for 48 hours. All compounds induced caspase 3 activity in cancer cells, but not fibroblasts.

Conclusions

- Treatment induced a dose-dependent increase in smooth, rounded, presumably mitotic cells as well as blebbed and rounded apoptotic cancer cells. Fibroblasts did not appear apoptotic after treatment.
- All compounds inhibited cell growth assessed by colony forming assay in cancer cells as well as in fibroblasts and increased mitotic arrest in both cancer cells and fibroblasts.
- Activation of caspase 3 in cancer cell lines but not in diploid fribroblasts suggests that these candidate compounds may be developable into cancer-selective drugs.

Acknowledgements

This research was supported in part by the University of Louisville Cancer Education Program NIH/NCI grant R25-CA134283.

LDH-A as a Potential Therapeutic Target for Non-small Cell Lung Cancer

Sabrina Schatzman,[1,2] Pankaj Seth, PhD,[4] Pawel Lorkiewicz, PhD,[1,2] Katherine Sellers, MS,[1,2] Teresa Fan, PhD.[1,2,3]

Departments of Chemistry[1], Center for Regulatory and Environmental Metabolomics[2], James Graham Brown Cancer Center[3]
University of Louisville
Department of Medicine, Divisions of Interdisciplinary Medicine and Biotechnology, Beth Israel Deaconess Medical Center, Harvard Medical School[4]

Abstract

We have characterized the metabolic effects of LDH-A knockdown (KD) in lung cancer metabolism with the use of shRNA in A549 NSCLC cells. $^{13}C_6$-Glucose and $^{13}C_5$-$^{15}N_2$-Glutamine were used as tracers to probe the perturbation of metabolic pathways induced by cells transduced with an anti LDH-A shRNA plasmid. The fate of the carbon and nitrogen isotopes through metabolic pathways was monitored by various analytical techniques including NMR, GC-MS, and FT-ICR-MS. LDH-A KD enhanced the concentration and enrichment of TCA cycle metabolites such as $^{13}C_2$ isotopologues of malate and fumarate when cells were given labeled glucose, supporting enhanced TCA cycle activity which can lead to increased oxidative phosphorylation. The fate of ^{13}C derived from glutamine suggests increased anaplerosis to the TCA cycle from glutaminase. The increased TCA cycle activity as a result of LDH-A knockdown may account for the previously observed increase in ROS production which, in turn, leads to cell death (2).

Introduction

Lung cancer is the leading cause of cancer related deaths in both men and women. Despite this alarming statistic, targeted therapies remain elusive. For this reason, there is a need to study cancer cell metabolism in order to find novel therapeutic approaches. Suppression of LDH-A, a monomor of tetrameric LDH, is thought to cause ROS-mediated apoptosis of non-small cell lung cancer (NSCLC) cells (2).

Lactate dehydrogenases (LDH) catalyze the following reaction:

Pyruvate + NADH →Lactate + NAD^+

There are two subunits (A and B) encoded by two separate genes(*LDH-A* and *LDH-B, respectively).*

Methods

$^{13}C_6$-Glc or $^{13}C_5$$^{15}N_2$-Gln were used as tracers. After an incubation period of 24 hours, cells were washed with cold PBS before quenching with acetonitrile.

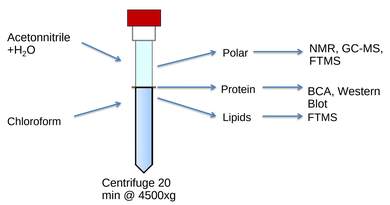

Figure 1. Separation of Metabolites by Centrifugation.

1. Effects on TCA Cycle

Enrichment of TCA cycle intermediates from $^{13}C_6$-Glc(A.) or $^{13}C_5$$^{15}N_2$-Gln(B.) Red dots in carbon skeletons denote ^{13}C. Important enzymes are labeled in bold. m+0 represents compound with no enrichement. Isotopologues are denoted by the addition of 13C or 15N units(from Glutamine) and are displayed as m+1, m+2, etc.

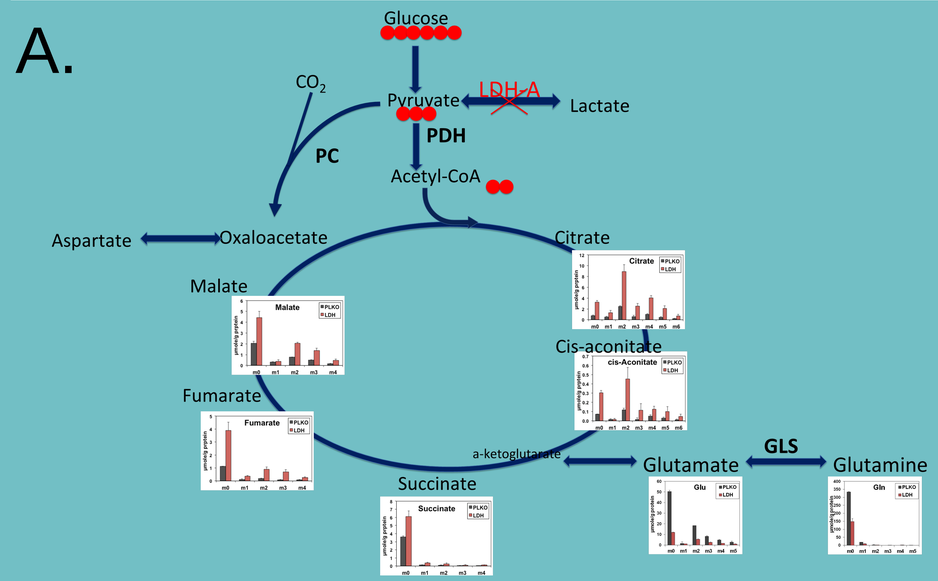

2. Effects on Nucleotides and Glutathione

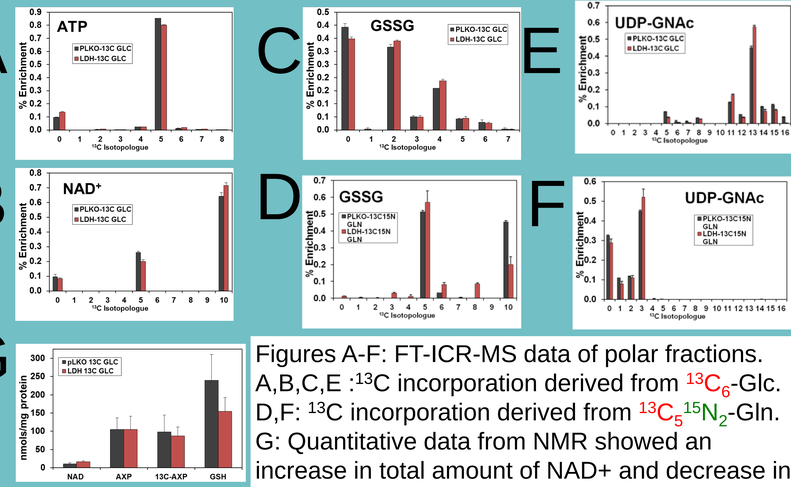

Figures A-F: FT-ICR-MS data of polar fractions. A,B,C,E :^{13}C incorporation derived from $^{13}C_6$-Glc. D,F: ^{13}C incorporation derived from $^{13}C_5$$^{15}N_2$-Gln. G: Quantitative data from NMR showed an increase in total amount of NAD+ and decrease in GSH. Increased labeling of NAD+ at m+10 suggests further incorporation of m+5 ribose derived from glucose. Depletion of GSH in LDH-A KD could be a result of the increase in ROS production

Conclusions

- Metabolomic analysis shows increased TCA cycle activity. This could explain the observed increase in ROS production in LDH-A KD cells.
- Increased labeling of TCA cycle intermediates derived from $^{13}C_5$$^{15}N_2$-Gln suggests an increase in glutaminase activity.

References

1. Fan, T.W., et al., *Altered regulation of metabolic pathways in human lung cancer discerned by (13)C stable isotope-resolved metabolomics (SIRM).* Mol Cancer, 2009. **8**: p. 41.
2. Seth P, Grant A, Tang J, Vinogradov E, Wang X, Lenkinski R, Sukhatme VP. On-target inhibition of tumor fermentative glycolysis as visualized by hyperpolarized pyruvate. Neoplasia 2011;13(1):60-71.

Acknowledgements

This work was supported by the University of Louisville Cancer Education Program NIH/NCI (R25-CA134283) and by funds to Seth laboratory from BIDMC and NCI.

Sustainable delivery of chemopreventives by biodegradable polymeric implants

R. Jennifer Siow[1], Farrukh Aqil[2], Radha Munagala[2] and Ramesh C. Gupta[1,2]

[1]Department of Pharmacology & Toxicology, [2]James Graham Brown Cancer Center, University of Louisville, Louisville, Kentucky

INTRODUCTION

- Phytochemicals have proven to be a valuable source of clinically useful drugs and cancer chemopreventive agents. However, poor oral bioavailability is a major obstacle to the use of natural chemopreventives in the prevention and treatment of cancer (Bansal et al., 2011).
- The use of subcutaneous polymeric implants bypasses the typical gut absorption and the liver first-pass effect and delivers these components systemically (Bansal et al., 2011; Gupta et al., 2012). Development of multi-layer "coated" implants has further improved this delivery system, reducing the initial burst and providing a more consistent drug release over time (Aqil et al., 2012).
- In this study, we describe the preparation of multilayer coated implants that can accommodate compounds of different physio-chemical properties. In an attempt to furnish more sustained release, reduce implant degradation time and increase drug release, polycaprolactone (PCL) in four lower-molecular weights (13K, 18K, 31K & 80K Da) were used to formulate coated implants. Drug release and implant degradation was monitored *in vitro.*
- We also analyzed the possible synergism between two chemopreventives known to inhibit tumor growth: anthocyanidins (colored compounds isolated from bilberry) and withaferin A (a terpenoid from the Ayurvedic herb "ashwagandha").

Degradation of PCL *In vitro*

RESULTS

In vitro release

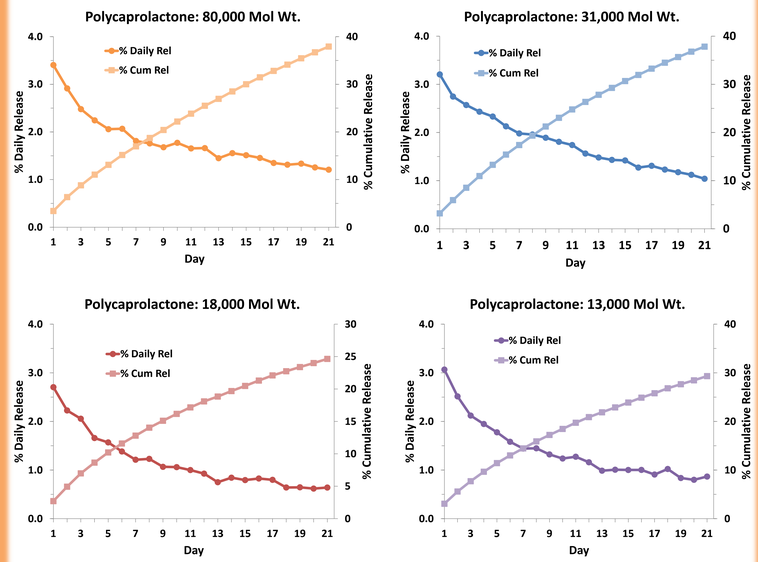

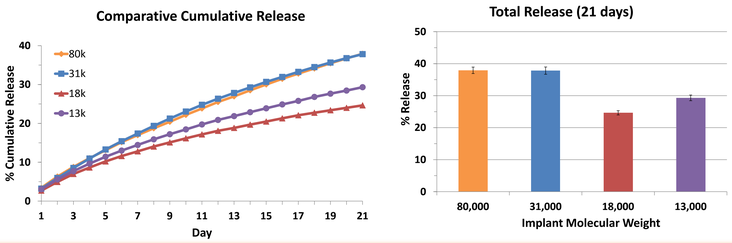

In vitro Release from Combination PCL implants

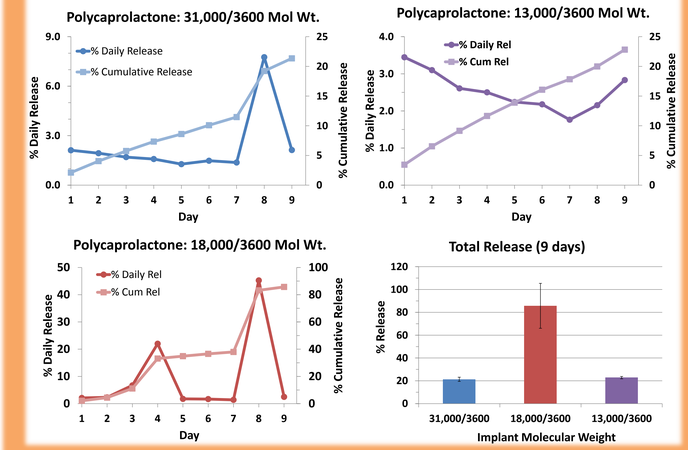

Tumor Xenograft

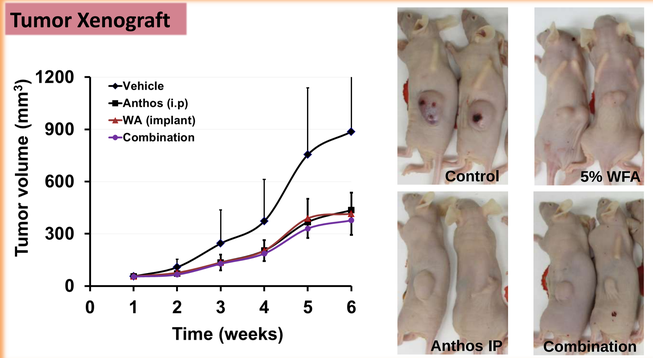

KEY FINDINGS

- Daily *in vitro* release varied with the mol. wt. of the implants. Cumulative release of curcumin from the 80K and 31K implants was found to be similar (~38%) and significantly higher than the release from the 18K and 13K implants (25% and 29%, respectively).
- No change in degradation rates was observed for the first 7-10 days, but a slight degradation in 13K and 18K implants was evident over the remaining days.
- Interestingly, 18K:3.6K PCL implants showed fast degradation resulting in dramatic high release (86%) *in vitro* in 9 days. However, only minor erosion of the implants was observed *in vivo* in the same period of time. The other two implant combinations released almost the same amount as released from the individual PCL implants (22-25%).
- Consistent with our previous findings, the treatments with the berry anthocyanidins and withaferin A individually inhibited tumor growth by 51% and 53%, respectively. The combination treatment showed only slightly increased inhibition of tumor growth (57%). No adverse reactions to the combination treatment were observed.

CONCLUSIONS

- ✓ Both 80K and 31K PCL implants had significantly higher release compared to 18K and 13K implants. As low molecular weight polymeric implants are expected to release more drug, another *in vitro* release study might be conducted to verify these findings.
- ✓ Although high release and rapid degradation was observed *in vitro* for the combination implants, these effects were not seen *in vivo*. This is perhaps due to the thin membrane formed around the implant. More studies with different combinations of PCL might find a combination that degrades rapidly in the body.
- ✓ Further testing at different doses is required to determine if anthocyanidins increase the effectiveness of sub-therapeutic doses of withaferin A.

MATERIALS & METHODS

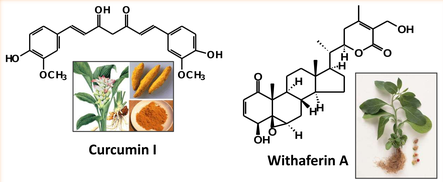

Phytocompounds and Polymers used in the study

Preparation of the blank implants: First, we prepared blank implants of PCL, mol. wt. 80K (Birmingham, AL, USA) and pluronic F68 (BASF Corporation, NJ, USA) in 9:1 (1.4 mm dia.) by extrusion method (Gupta *et al.,* 2012). Briefly, the polymers were dissolved in dichloromethane. After evaporation of the solvents under vacuum, the molten polymeric material was extruded through silastic tubing mould attached to a syringe. After a few minutes, the cylindrical implants were removed from the tubing, excised into desired lengths (~2.2 cm) and used for coating with polymer-drug solution.

Preparation of the implants: We chose different mol wt PCL ranging from 3.6K to 80K and three combinations of P-3.6K with P13K, P18K and P31K to determine the effect of different molecular weights on the release of test agent.

These blank implants were coated with 10-20% of P3.6K, P13K, P18K and P31K in dichloromethane with 10% curcumin in tetrahydrofuran. Withaferin A implants were prepared using P80 and 5% of withaferin A in dichloromethane. Thirty to 40 coatings were applied by dipping these blank implants with intermittent drying. After drying, the implants were excised into desired sizes. Sham implants were prepared essentially the same way in the absence of test agent.

***In vitro* release:** The rate of drug release was determined from 2 cm implants (except for P3.6K combinations, where we used 1.5 cm implants), in 20 ml glass vial containing 10 ml of release media (10% calf serum and 1% penicillin/streptomycin in PBS, pH 7.4) in a reciprocating shaker water bath (Julabo SW 23. Seelbach, Germany) at 37 C. The release media was changed every 24 hours. The presence of serum in the release medium mimicked the extracellular fluid composition *in vivo*. Curcumin concentration was measured with a spectrometer at 430 nm against a standard curve following the addition of ethanol (10%, final concentration) to ensure complete dissolution of drug (Gupta et al., 2012).

Lung cancer xenograft: Athymic nude mice were inoculated with human lung cancer A549 cells ($5x10^6$ cells), and then treated with either the native mixture of anthocyanidins from bilberry intraperitoneally (0.5 mg/mouse) on alternate days, or withaferin A via polymeric implants (5% w/w), or a combination of both treatments. Animals were weighed and tumor size was measured with a digital caliper weekly.

REFERENCES

Bansal S, Goel M, Aqil F, Vadhanam MV, Gupta RC. (2011). Advanced drug delivery systems of curcumin for cancer chemoprevention. Can Prev Res. 4:1158-1171.

Gupta RC, Bansal SS, Aqil F, Jeyabalan J, Cao P, Kausar H, Russell GK, Munagala R, Ravoori S, Vadhanam MV. (2012) Controlled-release systemic delivery - a new concept in cancer chemoprevention. Carcinogenesis. 33:1608-1615.

Aqil F, Jeyabalan J, Kausar H, Bansal SS, Sharma RJ, Singh IP, Vadhanam MV, Gupta RC (2012). Multi-layer polymeric implants for sustained release of chemopreventives. Can Lett. http://dx.doi.org/10.1016/j.canlet.2012.07.017, Epub.

Supported from: R25-CA134283 and Agnes Brown Duggan Endowment

Cancer Stem Cell induced Heterogeneity in Hepatocellular Cancer

Vanessa A. R. States, Yan Li, M.D., Ph.D., Su-Ping Li, M.S., Xuanyi Li, M.S., Dr. Robert C. G. Martin, M.D., Ph.D.
Department of Surgery
University of Louisville School of Medicine

Introduction

- **Current hepatocellular carcinoma (HCC) therapies:** liver resection, transplantation, hepatic arterial drug eluting bead therapy.
  - Targets rapidly dividing cells that make up tumor bulk
  - Recurrence free 3-year survival rates are <40%
- **Cancer Stem Cells (CSCs):** small, chemoresistant, subpopulation of cancer cells with stem-like properties
  - Capable of self-renewal and differentiation
  - Play a key role in tumor initiation, therapy failure and tumor relapse
  - Understanding the mechanisms of CSCs is imperative for the development of effective therapies
- **CSC Biomarkers:** EpCAM (CD326), CD90, CD44, and CD133 are widely accepted surface markers for the detection of pertential HCC CSCs.
- **Wnt/β-Catenin Pathway:** Regulates cell proliferation, fate specification, and migration in developing vertebrates
  - Improper activation associated with tumor formation and developmental defects
  - Suggested to be important for CSC maintenance and survival1

Hypothesis

a.) HCC cells are capable of dedifferentiating into CSCs under stressful conditions that reduce tumor bulk and

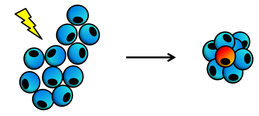

b.) Once ideal conditions are restored, the CSCs will differentiate into rapidly dividing HCC cells.

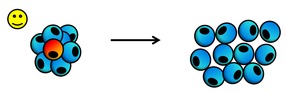

Experimental Design

In Vitro

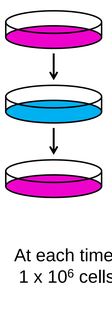

Grow Hepa1-6 cells in 5% FBS/RPMI media (“High Nutrient Media”, HNM) until they are ~90% confluent. Incubate at 37 C.

Replace medium with DMEM/F12 media with EGF & L-glut (“Serum-Free Media,” SFM.) Sphere formation should occur in 2-3 days.

Replace SFM with HNM. Cells should be growing evenly in 2-3 days.

At each time point, collect 1 x 10^6 cells per sample.

Perform indirect staining & analyze via flow cytometry.

At each time point, collect 2 x 10^6 cells per sample.

Perform western blot analysis

In Vivo

Hepa1-6 cells grown in HNM or SFM for 2-3 days

1 x 10^7 cells suspended in 100 μL injected into left flank of male BALB/c mouse

Cells dissociated into single cell suspension

Tumor formation (8 weeks)

Tumors excised and weighed

Results

Flow Cytometry

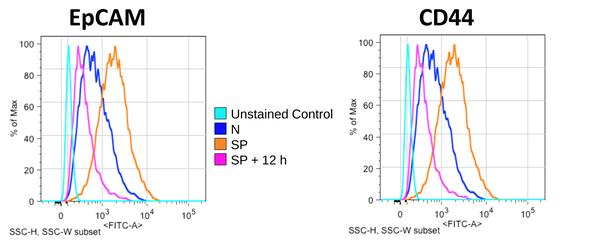

CD133

Treatment	Frequency of Parent	Median
N	95.38	3.5
SP	95.44	14
SP + 12 h	93.04	4.1

CD90

Treatment	Frequency of Parent	Median
N	0.066	1.3
SP	2.49	15
SP + 12 h	0.01	0.3

Figure 1. Surface marker analysis of HCC cells. Hepa1-6 cells were treated as indicated: normal culture medium (N), serum free medium (SP), serum free medium + 12 h normal culture media (SP +S).Sphere forming cells (SP) contained significantly higher amounts of CSC surface markers EpCAM, CD44, CD133, and CD90 than cells grown in normal culture medium (N).

HCC Mouse Model

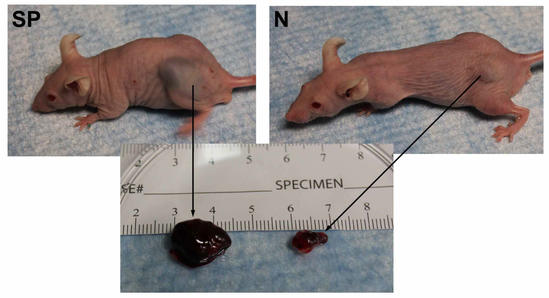

Figure 3. Nude mice inoculated with sphere-forming (SP) and non-sphere-forming HCC cells. SP cells demonstrated a significantly higher tumor proliferation rate compared to non-sphere (N). The tumor weights are as follows: 367mg(SP) 36, 89 15 (N). The values are expressed as means SD.

Conclusion

- There is a subpopulation of HCC cells that appear to be capable of de-differentiating into CSCs *in vitro*.
- CSCs spheres plays a key role in tumor formation and heterogeneity *in vivo*.
- Signaling pathways such as Wnt/β-catenin and TGFβ could potentially be related to cancer cell de-differentiation and CSCs activation.
- Further study is needed to understand CSC carcinogenesis and CSC signaling target(s) for cancer prevention and therapy.

Acknowledgements

Sponsored in part by NIH grant R25-CA134283.

Western Blot Analysis

EpCAM

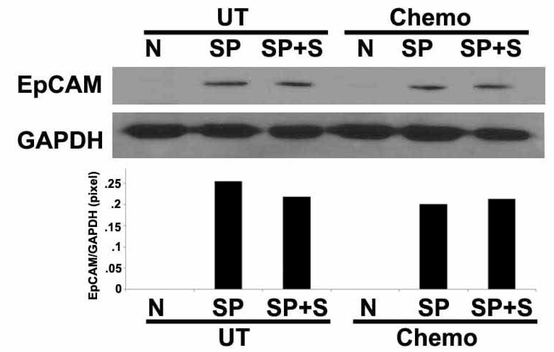

Wnt/β-Catenin Signaling Pathway Proteins

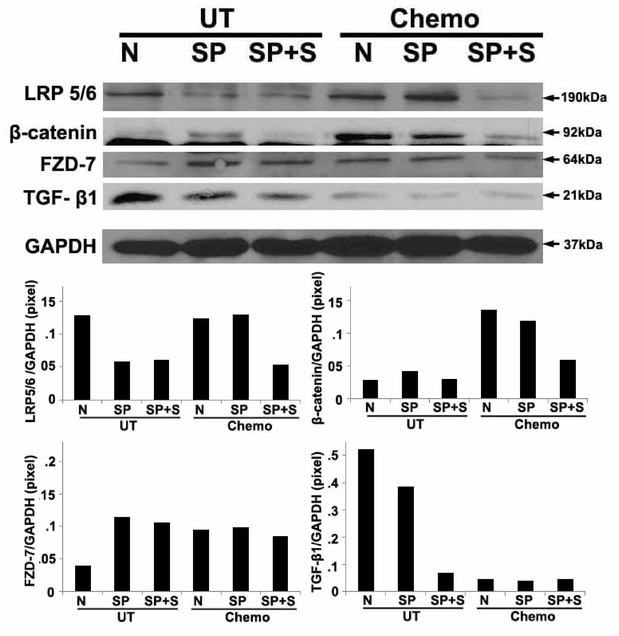

Figure 2. Protein analysis of HCC cells. Hepa1-6 cells were treated as indicated: normal culture medium (N + UT); serum free medium (SP + UT); serum free medium + 12 h normal culture medium (SP +S + UT); normal culture media with doxorubicin (N + Chemo); serum free medium with doxorubicin (SP + Chemo); serum free medium + 12 h normal culture media with doxorubicin (SP +S + Chemo); Western blot analysis was performed. Expression was semi-quantified by the pixel value using UN-SCAN-IT software. All the protein pixel values were normalized by GAPDH.